



Stable Möbius Bands from Isometrically Deformed Circular Helicoids

Vikash Chaurasia¹ · Eliot Fried¹

In memory of Jerald L. Ericksen

Received: 18 December 2022 / Accepted: 24 February 2023
© The Author(s) 2023, corrected publication 2023

Abstract

We consider the problem of producing a ruled Möbius band by subjecting an unstretchable, homogeneous, isotropic, elastic material surface in a circular helicoidal reference configuration to a deformation that is isometric and chirality preserving. We find that such a Möbius band is completely determined by the unit binormal of the Frenet frame of its midline, which must be a geodesic and must have uniform torsion inversely proportional to the pitch of the helicoidal reference configuration. Granted that the energy density of the material surface depends quadratically on the mean curvature of its deformed configuration, we show that the total energy stored in producing a ruled Möbius band as described reduces, in closed form and without approximation, to an integral over the midline of the Möbius band. We formulate and numerically solve a constrained variational problem for finding relative minima of the dimensionally reduced bending energy and construct corresponding stable Möbius bands. The only input parameter entering our variational problem is the number ν of turns in a helicoidal reference configuration. We only find solutions if ν exceeds a certain threshold, which we compute to machine precision. Above that threshold, an interplay between the operative constraints leads to a multiplicity of coexisting stable solutions with $n \geq 3$ half twists. For each $n \geq 3$, we construct an energetically optimal Möbius band which exhibits n -fold rotational symmetry. All other energy minima yield Möbius bands which lack symmetry. To our knowledge, this study contains the first examples of stable Möbius bands produced by isometrically deforming reference configurations that are not flat.

Keywords Material surface · Pure bending · Dimensional reduction · Lagrange multipliers · Local minima · Binormal scroll · Negative Gaussian curvature · Curve of constant torsion

Mathematics Subject Classification (2020) 74K25 · 74G15 · 49Q10 · 53A05 · 53Z05

✉ E. Fried
eliot.fried@oist.jp

V. Chaurasia
vikash.chaurasia2@oist.jp

¹ Mechanics and Materials Unit, Okinawa Institute of Science and Technology, Okinawa, 904-0495 Japan

1 Introduction

Our primary goal in this work is to supply provisional guidelines for producing Möbius bands from helicoidal templates. Candidates for such templates include coiled graphene nanoribbons like those synthesized by Daigle et al. [1] and helicoidal metalo-polymers like those synthesized by Fu et al. [2]. Helicoidal protein β -sheets described by Salemm [3] could also serve the intended purpose. It might also be possible to create suitable templates from DNA, prion proteins, collagen, chiral metal-organic frameworks, artificial proteins, or plasmonic nanoparticles.

We consider an idealized situation in which a ruled Möbius band is produced by subjecting an unstretchable, homogeneous, isotropic, elastic material surface in a circular helicoidal reference configuration to an isometric and chirality preserving deformation. We find that such a Möbius band must be generated by the unit binormal of its midline,¹ which must be a closed geodesic and have uniform torsion. Granted that the energy, per unit area, stored in bending a helicoidal reference configuration into a Möbius band depends quadratically on the mean curvature of the Möbius band and considering that a circular helicoid is a minimal surface and, thus, has zero mean curvature, we find that the total bending energy simplifies to an integral over the midline of the Möbius band. The integrand of the dimensionally reduced representation of the total bending energy is proportional to the square of the normal curvature of the midline of the Möbius band. Moreover, since the midline has uniform torsion, its squared normal curvature depends linearly on the square of the second derivative, with respect to arclength, of the unit binormal determining the Möbius band. The problem of finding a ruled Möbius band produced as described accordingly simplifies to the problem of determining the unit binormal of the corresponding midline.

After formulating a properly constrained variational problem for the unit binormal, we derive the corresponding first and second variation conditions. With a scaling in which lengths are measured relative to the length of the axis of a helicoidal reference configuration and energies are measured relative to an effective bending modulus that emerges during the derivation of the dimensionally reduced total bending energy, we find our problem has only one free parameter: the number, ν , of times a helicoidal reference configuration turns about its axis.

Using finite differences, we develop a second-order accurate scheme for constructing numerical solutions that satisfy discretized counterparts of our first and second variation conditions. Consistent with the intuitive expectation that it should not be possible to join the ends of a circular helicoid to form a Möbius band if the helicoid has too few turns, we find that a solution does not exist unless ν satisfies $\nu \geq 1.29$. The Möbius band determined by the solution corresponding to $\nu = 1.29$ is stable, has $n = 3$ half twists, and exhibits 3-fold rotational symmetry.

Also, we find one stable solution for each considered value of ν satisfying $1.30 \leq \nu < 1.40$ and two stable solutions for each considered value of ν satisfying $\nu \geq 1.40$. Each such solution produces an unknotted Möbius band that is stable in the sense that it delivers a local minimum of the bending energy. These Möbius bands typically lack symmetry. However, for each natural number $j \geq 2$, we discover particular values ν_j of ν which yield stable Möbius bands with $n = 2j + 1$ half twists and $(2j + 1)$ -fold rotational symmetry. Moreover, we find that the stable Möbius band with $n \geq 3$ half twists and n -fold rotational symmetry has lower dimensionless bending energy than every other stable Möbius band with the same number of half twists and is, thus, energetically optimal. Post-processing our numerical results for

¹Such a surface is called a binormal scroll.

$j = 1, \dots, 13$, we obtain heuristic approximations for the dimensionless bending energy F_j of the optimal Möbius band with $n = 2j + 1$ half twists and for v_j . We then use the latter approximation in conjunction with the interval halving to compute machine precision estimates of v_j up to $j = 100$. In so doing, we find that said approximation holds with at most 0.067% error.

Our numerical method does not rely on *a priori* symmetry assumptions of any kind. The energetically optimal Möbius bands with n half twists and n -fold rotational symmetry that we obtain arise naturally from our variational problem, which requires that bending energy be minimized while ensuring that the operative constraints and junction conditions are met. An alternative method designed to obtain only Möbius bands with n half twists and n -fold rotational symmetry might be more efficient than ours. However, such a method would not allow for the construction asymmetric competitors and, thus, would leave open the question of whether Möbius bands with n half twists and n -fold rotational symmetry are energetically optimal. Our numerical method also allows us to study the stability of solutions for the entire class of kinematically admissible perturbations rather than for the restricted subclass of perturbations that would otherwise be dictated within a method designed only for obtained solutions with symmetry.

In Sect. 2, we introduce our basic kinematical ingredients, derive the consequences of stipulating that the deformation from a circular helicoid to a ruled Möbius band be isometric and chirality preserving, and apply those consequences to show that any such Möbius band admits a parametrization entirely in terms of the unit binormal of the Frenet frame of its midline. In Sect. 3, we use the aforementioned parametrization to obtain a dimensional reduction of a simple but commonly used expression for bending energy. We then formulate a constrained variational problem, based on a dimensionless counterpart of the reduced bending energy, and derive the corresponding first and second variation conditions. In Sect. 4, we present discretized versions of the first and second variation conditions, constraints, and junction conditions. Our numerical results are presented in Sect. 5, where we describe local minima of the dimensionless bending energy and provide guidelines for constructing energetically optimal Möbius bands with n half twists and n -fold rotational symmetry for any choice of $n \geq 3$. We summarize and discuss our main findings, and we describe several possible areas of application of our work in Sect. 6. Calculations of several essential differential geometric quantities appear in the Appendix, and graphs of the left- and right-handed enantiomers of each energetically optimal Möbius band determined as an outcome of this study are provided as Supplemental Material.

2 Kinematics

2.1 Parameterizations of the Reference and Deformed Configurations

Consider a material surface in a (circular) helicoidal reference configuration \mathcal{H} with pitch $p \neq 0$, axis \mathcal{A} of length ℓ , and radius a . Given an orthonormal basis $\{\mathbf{e}_1, \mathbf{e}_2, \mathbf{e}_3\}$ with positive orientation, we parametrize \mathcal{H} by a mapping $\hat{\mathbf{x}}$ with the explicit form

$$\hat{\mathbf{x}}(s, v) = s\mathbf{e}_1 + v\mathbf{f}(s), \quad (1)$$

where \mathbf{f} is defined such that

$$\mathbf{f}(s) = \cos \frac{2\pi s}{p} \mathbf{e}_2 + \sin \frac{2\pi s}{p} \mathbf{e}_3, \quad (2)$$

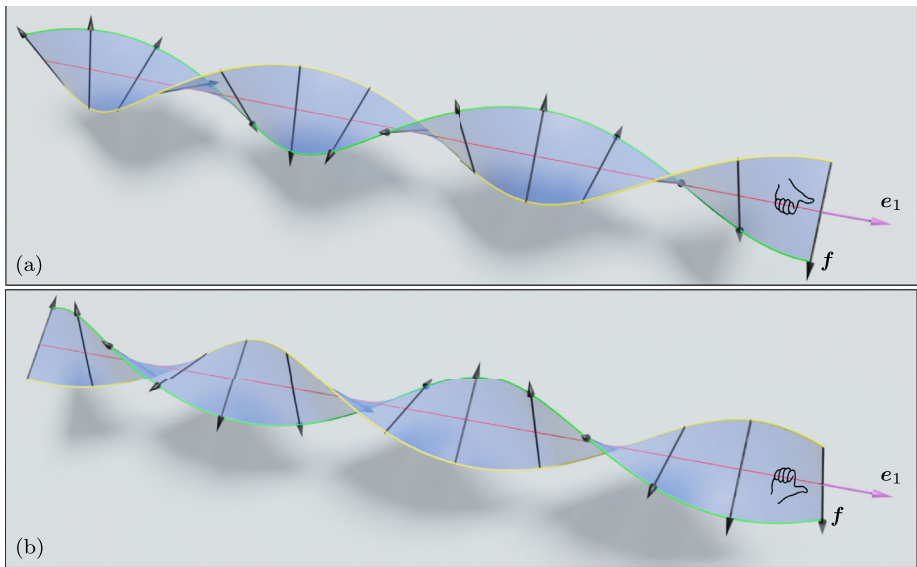


Fig. 1 (a) Illustration of a left-handed ($p < 0$) helicoidal reference configuration \mathcal{H} with $v = 1.70$ turns, as parametrized by the mapping $\hat{\mathbf{x}}$ defined in (1). (b) Illustration of the right-handed ($p > 0$) enantiomer of the helicoidal reference configuration \mathcal{H} shown in (a). For convenience, these helicoids are taken to be of unit width. The rulings are represented by black arrows, and a purple arrow is used to indicate the orientation \mathbf{e}_1 of the axis of each helicoid

and where each ordered pair (s, v) belongs to the rectangular parameter set

$$R = \{(s, v) : 0 \leq s \leq \ell, -a \leq v \leq a\}. \quad (3)$$

Thus, \mathcal{H} is right-handed or left-handed depending on whether p is positive or negative, respectively. Also, the dimensionless ratio

$$v = \frac{\ell}{|p|} > 0 \quad (4)$$

measures the number of times \mathcal{H} turns about its axis \mathcal{A} . Setting $v = 0$ in (1) shows that $\hat{\mathbf{x}}$ is defined so that s measures arclength along \mathcal{A} . Illustrations of left- and right-handed referential helicoids parametrized by (1), both with $v = 1.70$ turns, appear in Fig. 1.

A ruled Möbius band \mathcal{B} obtained by subjecting a helicoidal reference configuration \mathcal{H} to an isometric and chirality preserving deformation η can be parametrized by a mapping $\hat{\mathbf{y}}$ that is also defined on the parameter set R and has the general form

$$\hat{\mathbf{y}}(s, v) = \mathbf{d}(s) + v\mathbf{g}(s). \quad (5)$$

Without loss of generality, we stipulate that the point-valued mapping \mathbf{d} that enters (5), which is called the directrix of \mathcal{B} , parametrizes the closed midline \mathcal{C} of \mathcal{B} . The vector-valued mapping \mathbf{g} that enters (5), which is called the generatrix of \mathcal{B} , determines the orientation of a ruling through each point of \mathcal{C} . We assume that \mathbf{d} and \mathbf{g} are at least four times continuously differentiable. To ensure that the ends of \mathcal{A} are smoothly joined to form \mathcal{C} , we require that the values of \mathbf{d} and its first three derivatives agree at $s = 0$ and $s = \ell$:

$$\mathbf{d}(0) = \mathbf{d}(\ell), \quad \dot{\mathbf{d}}(0) = \dot{\mathbf{d}}(\ell), \quad \ddot{\mathbf{d}}(0) = \ddot{\mathbf{d}}(\ell), \quad \dddot{\mathbf{d}}(0) = \dddot{\mathbf{d}}(\ell). \quad (6)$$

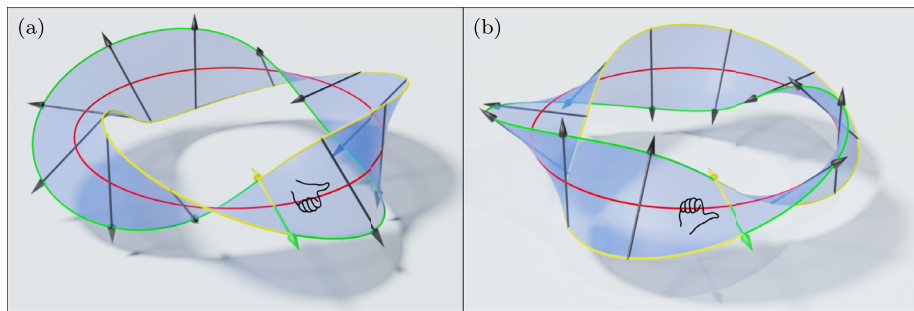


Fig. 2 (a) Illustration of a left-handed Möbius band with $n = 3$ half twists parametrized by augmenting the mapping $\hat{\mathbf{y}}$ defined in (5) with \mathbf{d} and \mathbf{g} given by (8) and (9). (b) Illustration of the right-handed enantiomer of the Möbius band shown in (a). As with the helicoids depicted in Fig. 1, these Möbius bands are taken to be of unit width and the rulings are represented by black arrows. The midline of each Möbius band is represented by a red curve. Antipodal terminal rulings are shown with green and yellow arrows

Moreover, to ensure that \mathcal{B} is nonorientable, we require the rulings at $s = 0$ and $s = \ell$ to be antipodal:

$$\mathbf{g}(0) = -\mathbf{g}(\ell). \quad (7)$$

Granted that the directrix \mathbf{d} and the generatrix \mathbf{g} satisfy (6)₁ and (7), the shape of the surface \mathcal{B} parametrized by (5) is independent of the particular values of $\mathbf{d}(0) = \mathbf{d}(\ell)$ and $\mathbf{g}(0) = -\mathbf{g}(\ell)$, which can therefore be chosen for convenience.

Figure 2 contains illustrations of left- and right-handed ruled Möbius bands, with $n = 3$ half twists and circular midlines of radius $\ell/2\pi$, obtained by prescribing \mathbf{d} and \mathbf{g} of (5) to be given by

$$\mathbf{d}(s) = \mathbf{d}_*(s) = \frac{\ell}{2\pi} \left(\cos \frac{2\pi s}{\ell} \mathbf{e}_2 + \sin \frac{2\pi s}{\ell} \mathbf{e}_3 \right), \quad 0 \leq s \leq \ell, \quad (8)$$

and

$$\mathbf{g}(s) = \mathbf{g}_*^\pm(s) = \cos \frac{3\pi s}{\ell} \mathbf{d}_*(s) \pm \sin \frac{3\pi s}{\ell} \mathbf{e}_1, \quad 0 \leq s \leq \ell, \quad (9)$$

where the minus and plus signs yield left- and right-handed enantiomers, respectively. It will become apparent that the Möbius bands depicted in Fig. 2 cannot be obtained by isometrically deforming helicoidal reference configurations and, thus, do not correspond to solutions of the problem considered in this study.

2.2 Consequences of Isometry and Chirality Preservation

Under a deformation η from \mathcal{H} to \mathcal{B} , each material point $\mathbf{x} = \hat{\mathbf{x}}(s, \nu)$ on \mathcal{H} is mapped to a unique point

$$\mathbf{y} = \hat{\mathbf{y}}(s, \nu) = \eta(\hat{\mathbf{x}}(s, \nu)) \quad (10)$$

of \mathcal{B} . Since we have assumed that the directrix \mathbf{d} of \mathcal{B} parametrizes the midline \mathcal{C} of \mathcal{B} , we see from (1), (5), and (10) that

$$\mathbf{d}(s) = \eta(s\mathbf{e}_1), \quad 0 \leq s \leq \ell. \quad (11)$$

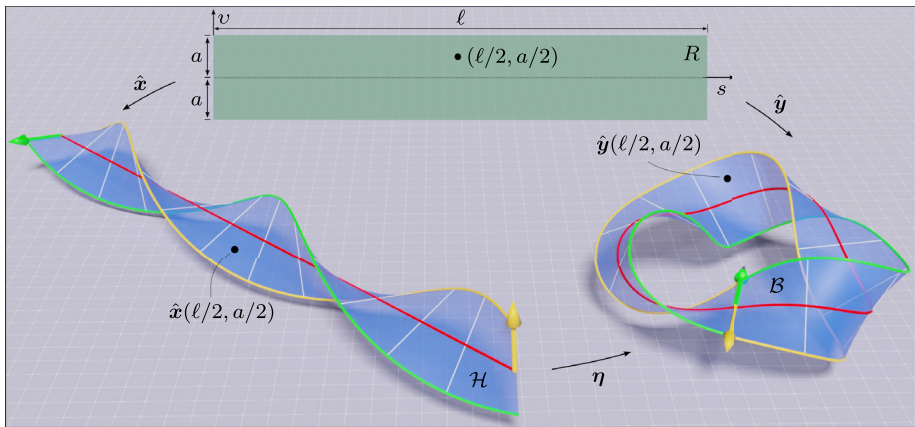


Fig. 3 Illustration of a Möbius band \mathcal{B} with $n = 3$ half twists and 3-fold rotational symmetry produced by subjecting a right-handed helicoidal reference configuration \mathcal{H} , with $v = 1.29$ turns and length-to-radius aspect ratio $\ell/a = 20.0$, to an isometric and chirality preserving deformation η . The axis \mathcal{A} of \mathcal{H} and the midline of \mathcal{B} are depicted by red curves, and white lines depict the rulings of both surfaces. Also, the edges of \mathcal{H} are shown in yellow and green. Due to the nonorientability of \mathcal{B} , the edges of \mathcal{H} join smoothly to form the edge of \mathcal{B} . Moreover, the terminal rulings of \mathcal{H} , depicted by green and yellow arrows, form an antipodal junction. The set R upon which the respective parametrizations \hat{x} and \hat{y} of \mathcal{H} and \mathcal{B} are defined is also shown, in green. Also shown are the location $\hat{x}(\ell/2, a/2)$ on \mathcal{H} and $\hat{y}(\ell/2, a/2) = \eta(\hat{x}(\ell/2, a/2))$ on \mathcal{B} of the material point associated with the particular choice $(s, v) = (\ell/2, a/2)$

Hence, η maps the axis \mathcal{A} of \mathcal{H} onto \mathcal{C} . Since \mathcal{A} is a geodesic of \mathcal{H} and since geodesics are preserved under isometric deformations, \mathcal{C} must be a geodesic of \mathcal{B} . An illustration of an isometric deformation η from a helicoidal reference configuration \mathcal{H} with $v = 1.29$ turns to a Möbius band \mathcal{B} with $n = 3$ half twists and 3-fold rotational symmetry appears in Fig. 3.

To qualify as an isometric deformation, η must preserve the length of any curve connecting any two points on \mathcal{H} and, thus, bend \mathcal{H} into \mathcal{B} entirely without stretching. Differentiating the identity $\hat{y}(s, v) = \eta(\hat{x}(s, v))$ with respect to s and v , we consequently infer that the corresponding metric coefficients of \mathcal{H} and \mathcal{B} must match for each (s, v) in R . In Appendix A.1, we show that those metric requirements are met if and only if the directrix \mathbf{d} and generatrix \mathbf{g} of \mathcal{B} satisfy

$$|\dot{\mathbf{d}}| = 1, \quad |\mathbf{g}| = 1, \quad \dot{\mathbf{d}} \cdot \mathbf{g} = 0, \quad \dot{\mathbf{d}} \cdot \dot{\mathbf{g}} = 0, \quad \text{and} \quad |\dot{\mathbf{g}}| = \frac{2\pi}{|p|}. \quad (12)$$

Immediately useful consequences of (12) include

$$\dot{\mathbf{g}} \cdot \mathbf{g} = 0 \quad \text{and} \quad |\mathbf{g} \times \dot{\mathbf{g}}| = \frac{2\pi}{|p|}. \quad (13)$$

While (13)₁ stems from differentiating (12)₂, (13)₂ can be confirmed with reference to (12)₅ and (13)₁. By (12)₃ and (12)₄, $\dot{\mathbf{d}}$ must be orthogonal to both \mathbf{g} and $\dot{\mathbf{g}}$. Referring to (13), we thus find that $\dot{\mathbf{d}}$ must be determined by \mathbf{g} through

$$\dot{\mathbf{d}} = \pm \frac{p}{2\pi} \mathbf{g} \times \dot{\mathbf{g}}. \quad (14)$$

Since, by (12)₅ and (13)₁, $\dot{\mathbf{g}} \times (\mathbf{g} \times \dot{\mathbf{g}}) = 4\pi^2 \mathbf{g} / p^2$, we find from (14) that \mathbf{g} can be expressed as

$$\mathbf{g} = \pm \frac{p}{2\pi} \dot{\mathbf{g}} \times \dot{\mathbf{d}}. \quad (15)$$

An isometric deformation η from \mathcal{H} to \mathcal{B} preserves the chirality of \mathcal{H} if and only if, as arclength increases, the rulings of \mathcal{B} turn around its midline \mathcal{C} in the same way that the rulings of \mathcal{H} turn around its axis \mathcal{A} . As arclength along \mathcal{C} increases, the rule vector of a helicoidal reference configuration \mathcal{H} with parametrization (1) rotates anticlockwise or clockwise about \mathcal{A} depending on the sign of the pitch p . The rotation about \mathcal{A} is clockwise or anticlockwise depending on whether \mathcal{H} is left-handed ($p < 0$) or right-handed ($p > 0$). Hence, \mathcal{B} has the same chirality as \mathcal{H} only if

$$\dot{\mathbf{d}} \cdot (\mathbf{g} \times \dot{\mathbf{g}}) = \mathbf{e}_1 \cdot (\mathbf{f} \times \dot{\mathbf{f}}) = \frac{2\pi}{p} \quad (16)$$

and, thus, only if the plus sign must prevail in (14) and (15), giving

$$\dot{\mathbf{d}} = \frac{p}{2\pi} \mathbf{g} \times \dot{\mathbf{g}} \quad \text{and} \quad \mathbf{g} = \frac{p}{2\pi} \dot{\mathbf{g}} \times \dot{\mathbf{d}}. \quad (17)$$

In view of (5) and (12)₁₋₃, $\mathbf{n} = \mathbf{g} \times \dot{\mathbf{d}}$ defines a unit normal to \mathcal{B} at each point of \mathcal{C} . With reference to (12)₂, (13)₁, and (17)₁, we find that

$$\mathbf{n} = -\frac{p}{2\pi} \dot{\mathbf{g}}. \quad (18)$$

Invoking (12)₅, we confirm that the right-hand of (18) is of unit magnitude. With (18), we may rewrite (17) as

$$\dot{\mathbf{d}} = \mathbf{n} \times \mathbf{g} \quad \text{and} \quad \mathbf{g} = \dot{\mathbf{d}} \times \mathbf{n}. \quad (19)$$

The positively-oriented orthonormal triad $\{\dot{\mathbf{d}}, \mathbf{n}, \mathbf{g}\}$ can thus be recognized as the Darboux frame of the midline \mathcal{C} of \mathcal{B} . Since \mathcal{C} is a geodesic of \mathcal{B} , its vector curvature $\ddot{\mathbf{d}}$ must be normal to \mathcal{B} and, thus, must be given by

$$\ddot{\mathbf{d}} = k\mathbf{n}, \quad (20)$$

where the normal curvature k of \mathcal{C} is given by

$$k = \ddot{\mathbf{d}} \cdot \mathbf{n}. \quad (21)$$

Next, noticing that, by (18)–(20),

$$(\dot{\mathbf{d}} \times \ddot{\mathbf{d}}) \cdot \ddot{\mathbf{d}} = k\mathbf{g} \cdot (\dot{\mathbf{d}}\mathbf{n} + k\dot{\mathbf{n}}) = k^2 \mathbf{g} \cdot \dot{\mathbf{n}} = -|\ddot{\mathbf{d}}|^2 \mathbf{n} \cdot \dot{\mathbf{g}} = \frac{2\pi}{p} |\ddot{\mathbf{d}}|^2, \quad (22)$$

we find that the torsion τ of \mathcal{C} must be uniform and is determined by the pitch p of \mathcal{H} through

$$\tau = \frac{(\dot{\mathbf{d}} \times \ddot{\mathbf{d}}) \cdot \ddot{\mathbf{d}}}{|\ddot{\mathbf{d}}|^2} = \frac{2\pi}{p}. \quad (23)$$

Thus, in particular, τ is positive (negative) for a right-handed (left-handed) referential helioid \mathcal{H} . From (18) and the definition $\tau_g = \dot{\mathbf{n}} \cdot \mathbf{g} = -\mathbf{n} \cdot \dot{\mathbf{g}}$ of the geodesic torsion of \mathcal{C} , we also find that

$$\tau_g = \frac{2\pi}{p} = \tau. \quad (24)$$

As a consequence of (24), the angle between the Darboux and Frenet frames of \mathcal{C} is fixed. With this in mind, we notice from (20) that the unit normal \mathbf{n} of the Darboux frame of \mathcal{C} must also serve as the unit normal of the Frenet frame of \mathcal{C} and, accordingly, that the unit binormal \mathbf{b} of the Frenet frame of \mathcal{C} must be given by

$$\mathbf{b} = \dot{\mathbf{d}} \times \mathbf{n} = \mathbf{g}. \quad (25)$$

Invoking Fenchel's [4] definitions of the Frenet frame and the curvature,² we thus infer that the generatrix \mathbf{g} of \mathcal{B} is equal to the unit binormal \mathbf{b} of the midline \mathcal{C} of \mathcal{B} . By (25), the normalization which \mathbf{b} must satisfy to qualify as the unit normal of \mathcal{C} , namely

$$|\mathbf{b}| = 1, \quad (26)$$

is sufficient to ensure that (12)₂ holds. Using (25) in (12)₅, we deduce that \mathbf{b} must satisfy an additional normalization of the form

$$|\dot{\mathbf{b}}| = \frac{2\pi}{|p|}. \quad (27)$$

Integrating the consequence

$$\dot{\mathbf{d}} = \frac{p}{2\pi} \mathbf{b} \times \dot{\mathbf{b}} \quad (28)$$

of using (25) in (17)₁, we next conclude that the directrix \mathbf{d} of \mathcal{C} must be determined as a functional of the unit binormal \mathbf{b} of the Frenet frame of \mathcal{C} through

$$\mathbf{d}(s) = \mathbf{d}(0) + \frac{p}{2\pi} \int_0^s \mathbf{b}(\varsigma) \times \dot{\mathbf{b}}(\varsigma) \, d\varsigma, \quad 0 \leq s \leq \ell, \quad (29)$$

where, as previously noted, $\mathbf{d}(0)$ can be chosen arbitrarily.³ Furthermore, using (25) and (29) in (5), we obtain the parametrization $\hat{\mathbf{y}}$ of \mathcal{B} in the form

$$\hat{\mathbf{y}}(s, v) = \mathbf{d}(0) + \frac{p}{2\pi} \int_0^s \mathbf{b}(\varsigma) \times \dot{\mathbf{b}}(\varsigma) \, d\varsigma + v\mathbf{b}(s), \quad (s, v) \in R, \quad (30)$$

and, thus, that \mathcal{B} must be a binormal scroll with midline \mathcal{C} of uniform torsion $\tau = 2\pi/p$.

²According to Adams et al. [5], Fenchel's [4] definitions of the Frenet frame and curvature allow the curvature to be negative or to vanish and are meaningful as long as the arclength derivatives of the unit tangent and unit binormal do not vanish simultaneously. (For the conventional definitions of those objects, the curvature of \mathcal{C} is equal to $|k|$ and it follows from (20) and (24) that the angle between the Frenet and Darboux frames may be chosen equal to either 0 or π .) We allow the normal curvature k to vanish at isolated points of \mathcal{C} . The vector curvature $\dot{\mathbf{d}}$ defined in (20) will therefore vanish at any point of \mathcal{C} at which k vanishes. Regardless, we see from (12)₅ and (25) that $\dot{\mathbf{b}}$ never vanishes. Fenchel's [4] definitions of the Frenet frame and curvature therefore apply in the present context.

³In arriving at (29), we have recovered Koenigs' [6] representation for a space curve of uniform torsion.

2.3 Explicit Form of the Deformation from \mathcal{H} to \mathcal{B}

Let \mathbf{o} denote the reference placement of the material point corresponding to the parameter pair $(s, v) = (0, 0)$, and let $x_i = (\mathbf{x} - \mathbf{o}) \cdot \mathbf{e}_i$, $i = 1, 2, 3$. Referring to (1) and (2), we thus see the Cartesian coordinates (x_1, x_2, x_3) of a point $\mathbf{x} = \hat{\mathbf{x}}(s, v)$ on a helicoidal reference configuration \mathcal{H} must satisfy

$$x_1 = s \quad \text{and} \quad x_2 \cos \frac{2\pi x_1}{p} + x_3 \sin \frac{2\pi x_1}{p} = v, \quad (s, v) \in R. \quad (31)$$

In view of (1), (10), (30), and (31), we infer that the deformation $\boldsymbol{\eta}$ takes the material point $\mathbf{x} = \hat{\mathbf{x}}(s, v)$ on \mathcal{H} with Cartesian coordinates (x_1, x_2, x_3) to the point \mathbf{y} on \mathcal{B} given by

$$\mathbf{y} = \boldsymbol{\eta}(\mathbf{x}) = \mathbf{d}(0) + \frac{p}{2\pi} \int_0^{x_1} \mathbf{b}(s) \times \dot{\mathbf{b}}(s) \, ds + \left(x_2 \cos \frac{2\pi x_1}{p} + x_3 \sin \frac{2\pi x_1}{p} \right) \mathbf{b}(x_1). \quad (32)$$

2.4 Closure and Junction Conditions

Using (29) to evaluate the difference $\mathbf{d}(\ell) - \mathbf{d}(0)$, we see that the closure condition (6)₁ takes the form

$$\int_0^\ell \mathbf{b} \times \dot{\mathbf{b}} \, ds = \mathbf{0}. \quad (33)$$

As a first step toward considering the implications of (6)₂₋₄, we use (25) to recast the antipodal junction condition (7) in terms of \mathbf{b} , giving

$$\mathbf{b}(0) = -\mathbf{b}(\ell). \quad (34)$$

Next, we differentiate (28) to yield:

$$\ddot{\mathbf{d}} = \frac{p}{2\pi} \mathbf{b} \times \ddot{\mathbf{b}}, \quad \ddot{\mathbf{d}} = \frac{p}{2\pi} (\mathbf{b} \times \ddot{\mathbf{b}} + \dot{\mathbf{b}} \times \dot{\mathbf{b}}). \quad (35)$$

Using (28) and (35) in (6)₂₋₄ and taking advantage of (34), we obtain the conditions:

$$\left. \begin{aligned} \mathbf{b}(0) \times (\dot{\mathbf{b}}(0) + \dot{\mathbf{b}}(\ell)) &= \mathbf{0}, \\ \mathbf{b}(0) \times (\ddot{\mathbf{b}}(0) + \ddot{\mathbf{b}}(\ell)) &= \mathbf{0}, \\ \mathbf{b}(0) \times (\dot{\mathbf{b}}(0) + \dot{\mathbf{b}}(\ell)) + \dot{\mathbf{b}}(0) \times \ddot{\mathbf{b}}(0) - \dot{\mathbf{b}}(\ell) \times \ddot{\mathbf{b}}(\ell) &= \mathbf{0}. \end{aligned} \right\} \quad (36)$$

Since $\mathbf{b}(0)$ can be chosen arbitrarily without influencing the shape of \mathcal{B} , we see from (36)_{1,2} that $\dot{\mathbf{b}}$ and $\ddot{\mathbf{b}}$ must satisfy antipodal junction conditions:

$$\dot{\mathbf{b}}(0) = -\dot{\mathbf{b}}(\ell), \quad \ddot{\mathbf{b}}(0) = -\ddot{\mathbf{b}}(\ell). \quad (37)$$

Using (37) to simplify (36)₃ and relying again on the arbitrary nature of $\mathbf{b}(0)$, we find that $\ddot{\mathbf{b}}$ must also satisfy an antipodal junction condition:

$$\ddot{\mathbf{b}}(0) = -\ddot{\mathbf{b}}(\ell). \quad (38)$$

2.5 Number of Half Twists in a Ruled Möbius Band

Granted that \mathbf{b} satisfies the antipodal junction conditions (34), (37), and (38), a theorem due to Călugăreanu [7] can be used to determine how many half twists are in a Möbius band \mathcal{B} with midline \mathcal{C} and parametrization $\hat{\mathbf{y}}$ of the form (30). If \mathcal{B} is an unknot, we find that its number n of half twists is given by

$$n = 2(\nu + w), \quad (39)$$

where

$$w = \frac{1}{2\pi} \left| \int_0^\ell \int_0^\ell \frac{(\dot{\mathbf{d}}(s) \times \dot{\mathbf{d}}(\zeta)) \cdot (\mathbf{d}(s) - \mathbf{d}(\zeta))}{|\mathbf{d}(s) - \mathbf{d}(\zeta)|^3} d\zeta ds \right| \quad (40)$$

measures the writhe of \mathcal{C} .⁴ Since (29) can be used to express w in terms of \mathbf{b} , (39) determines n in terms of \mathbf{b} . If \mathcal{B} is a knot, then (39) changes to $n = 2(\nu + w - c)$, where c measures the number of times that \mathcal{C} crosses over itself.⁵

3 Energetics

3.1 Dimensional Reduction of the Bending Energy

The energy stored in isometrically deforming a homogeneous, isotropic, elastic material surface can include only contributions due to bending. Since the Gaussian curvature is preserved under an isometric deformation $\boldsymbol{\eta}$ and since the mean curvature of a circular helicoidal reference configuration \mathcal{H} vanishes, the bending energy density of a ruled Möbius band \mathcal{B} obtained from a smooth, isometric, chirality preserving deformation $\boldsymbol{\eta}$ of any such \mathcal{H} can depend only on the mean curvature H of \mathcal{B} . For simplicity, we take that dependence to be quadratic. The resistance to bending is then characterized by a constant modulus $\mu > 0$ and the total energy E stored in bending \mathcal{H} to \mathcal{B} has the form

$$E = 2\mu \int_{\mathcal{B}} H^2 da. \quad (41)$$

To convert (41) to an integral over the parameter set R defined in (3), we determine the first and second fundamental forms \mathbf{I} and \mathbf{II} of \mathcal{B} . With reference to the explicit representation (30) of the parametrization $\hat{\mathbf{y}}$ of \mathcal{B} and to the normalization conditions (26) and (27) that apply to \mathbf{b} , we show in Appendix A.2 that

$$\mathbf{I} = \begin{bmatrix} J^2 & 0 \\ 0 & 1 \end{bmatrix} \quad \text{and} \quad \mathbf{II} = \begin{bmatrix} k_J & -2\pi/p_J \\ -2\pi/p_J & 0 \end{bmatrix}, \quad (42)$$

where J , defined according to

$$J(v) = \sqrt{1 + \frac{4\pi^2 v^2}{p^2}}, \quad -a \leq v \leq a, \quad (43)$$

⁴The writhe w connotes the extent to which a curve is coiled. While the torsion τ and the writhe w of a curve can be altered without changing the topology of the curve, their sum, as proven by Călugăreanu [7], remains preserved if the topology of the curve is constrained to be invariant.

⁵See Kleitman [8] for a definition of the crossing number c of a knot.

is the Jacobian needed to convert the area element da of \mathcal{B} to the area element $ds dv$ of the parameter set R . From (42), we obtain the mean curvature H of \mathcal{B} in the form

$$H(\hat{\mathbf{y}}(s, v)) = \frac{1}{2} \text{tr}(\mathbf{l}^{-1}(v) \mathbf{II}(s, v)) = \frac{k(s)}{2J(v)}, \quad (s, v) \in R, \quad (44)$$

and, thus, is a multiplicatively separable function of s and v .

Since the integrand of the double integral arising from using (43) and (44) in (41) is also a multiplicatively separable function of s and v and the parameter set R is rectangular, E splits into the product

$$E = I_1 I_2, \quad (45)$$

with

$$I_1 = \frac{\ell}{2} \int_0^\ell k^2 ds, \quad I_2 = \frac{\mu}{\ell} \int_{-a}^a \frac{dv}{J}. \quad (46)$$

With reference to (43), we notice that I_2 can be evaluated explicitly. Introducing

$$\alpha = \frac{\mu p}{\pi \ell} \operatorname{arcsinh} \frac{2\pi a}{p}, \quad (47)$$

we thus obtain a dimensional reduction, in closed form, of E :

$$E = \frac{\alpha \ell}{2} \int_0^\ell k^2 ds. \quad (48)$$

The energy stored in bending a circular helicoidal reference configuration \mathcal{H} with pitch p , length ℓ , and radius a into a ruled Möbius band \mathcal{B} with midline \mathcal{C} is therefore equivalent to the energy stored in bending an inextensible elastica of length ℓ and effective bending stiffness $\alpha \ell$ into a space curve with the shape of \mathcal{C} . To acquire some insight regarding α , which can be identified as a characteristic measure of bending energy, let μ and the width-to-length ratio $2a/\ell$ of \mathcal{H} be fixed. We then see from (47) that

$$\frac{\alpha \ell}{2\mu a} = \frac{\operatorname{arcsinh} m}{m} \sim \begin{cases} 1, & |m| \ll 1, \\ \frac{\log |m|}{|m|}, & |m| \gg 1, \end{cases} \quad (49)$$

where m defined by

$$m = \frac{2\pi a}{p} \quad (50)$$

can be recognized as the slope of the helical edge of \mathcal{H} . Granted that μ and $2a/\ell$ are fixed, we thus see from (49) that: (i) α is insensitive to m for sufficiently small values of $|m|$; (ii) since

$$1 \leq \log |m| < |m|^{1/2} \quad \text{for} \quad |m| \geq e, \quad (51)$$

α decays more rapidly than $|m|^{-1/2}$ but more slowly than $|m|^{-1}$ as $|m|$ increases for sufficiently large values of $|m|$; (iii) since

$$\frac{\operatorname{arcsinh} m}{m} \geq \frac{1}{\sqrt{1+m^2}}, \quad -\infty < m < \infty, \quad (52)$$

where equality is achieved if and only if $m = 0$, it follows that

$$\frac{d}{dm} \left(\frac{\operatorname{arcsinh} m}{m} \right) = \frac{1}{m} \left(\frac{1}{\sqrt{1+m^2}} - \frac{\operatorname{arcsinh} m}{m} \right) \rightarrow \begin{cases} > 0, & m < 0, \\ = 0, & m = 0, \\ < 0, & m > 0, \end{cases} \quad (53)$$

and, thus, that $\alpha\ell/2\mu a$ increases monotonically with m for $m < 0$ and decreases monotonically with m for $m > 0$.

Toward formulating a variational problem for determining admissible choices of the unit binormal \mathbf{b} of the midline \mathcal{C} of \mathcal{B} , we express the dimensionally reduced expression (48) for bending energy E of \mathcal{B} as a functional of \mathbf{b} . Specifically, from (35)₁ and the consequence

$$\begin{aligned} |\mathbf{b} \times \ddot{\mathbf{b}}|^2 &= |\mathbf{b}|^2 |\ddot{\mathbf{b}}|^2 - (\mathbf{b} \cdot \ddot{\mathbf{b}})^2 = |\ddot{\mathbf{b}}|^2 - \left(\overline{\mathbf{b} \cdot \dot{\mathbf{b}}} - |\dot{\mathbf{b}}|^2 \right)^2 = |\ddot{\mathbf{b}}|^2 - \left(\frac{1}{2} \overline{|\dot{\mathbf{b}}|^2} - \frac{4\pi^2}{p^2} \right)^2 \\ &= |\ddot{\mathbf{b}}|^2 - \frac{16\pi^4}{p^4} \end{aligned} \quad (54)$$

of (26) and (27), we find that the square $k^2 = |\ddot{\mathbf{d}}|^2$ of the normal curvature k of \mathcal{C} can be expressed as

$$k^2 = \frac{p^2}{4\pi^2} |\ddot{\mathbf{b}}|^2 - \frac{4\pi^2}{p^2}. \quad (55)$$

Using (55) in (48) and invoking the definition (4) of the number ν of turns of \mathcal{H} , we thus obtain an alternative representation for the total energy E stored in bending \mathcal{H} to \mathcal{B} :

$$E = \frac{\alpha\ell^3}{8\pi^2\nu^2} \int_0^\ell |\ddot{\mathbf{b}}|^2 ds - 2\alpha\pi^2\nu^2. \quad (56)$$

3.2 Scaling

We adopt a scaling whereby lengths are measured relative to the length ℓ of the axis \mathcal{A} of a helicoidal reference configuration \mathcal{H} and energies are measured relative to the parameter α that emerges as a natural offshoot in the derivation of the dimensional reduced version (48) of the bending energy E . This is accomplished by defining dimensionless counterparts x and \mathbf{u} of the arclength s and the unit binormal \mathbf{b} through

$$x = \frac{s}{\ell} \quad \text{and} \quad \mathbf{u}(x) = \mathbf{b}(\ell x), \quad 0 \leq x \leq 1, \quad (57)$$

and defining a dimensionless counterpart F of the bending energy E through

$$F = \frac{E}{\alpha} = \frac{1}{8\pi^2\nu^2} \int_0^1 |\mathbf{u}''|^2 dx - 2\pi^2\nu^2, \quad (58)$$

where a prime signifies differentiation with respect to x .

With the change of variables (57), the parametrization (29) of midline \mathcal{C} of \mathcal{B} takes the form

$$\mathbf{d}(s, v) = \mathbf{d}(0) + \frac{p}{2\pi} \int_0^{s/\ell} \mathbf{u}(\xi) \times \mathbf{u}'(\xi) d\xi, \quad 0 \leq s \leq \ell. \quad (59)$$

Accordingly, the parametrization (30) of \mathcal{B} takes the form

$$\hat{\mathbf{y}}(s, v) = \mathbf{d}(0) + \frac{p}{2\pi} \int_0^{s/\ell} \mathbf{u}(\xi) \times \mathbf{u}'(\xi) d\xi + v\mathbf{u}(s/\ell), \quad (s, v) \in R. \quad (60)$$

Moreover, the normalization conditions (26) and (27) are converted to

$$|\mathbf{u}| = 1 \quad \text{and} \quad |\mathbf{u}'| = 2\pi v, \quad (61)$$

the closure condition (33) reads

$$\int_0^1 \mathbf{u} \times \mathbf{u}' dx = \mathbf{0}, \quad (62)$$

and the antipodal junction conditions (34), (37), and (38) become

$$\left. \begin{aligned} \mathbf{u}(0) &= -\mathbf{u}(1), & \mathbf{u}'(0) &= -\mathbf{u}'(1), \\ \mathbf{u}''(0) &= -\mathbf{u}''(1), & \text{and } \mathbf{u}'''(0) &= -\mathbf{u}'''(1). \end{aligned} \right\} \quad (63)$$

3.3 Variational Problem

In seeking admissible local minima of the dimensionless energy functional F defined in (58), we interpret the normalization conditions (61) and the closure condition (62) as constraints and introduce corresponding Lagrange multipliers ρ , λ , and $\boldsymbol{\gamma}$ that penalize deviations from the constraints. Since (61) are pointwise conditions, the scalar multipliers ρ and λ generally depend on the dimensionless arclength x . Since (62) is a global condition, $\boldsymbol{\gamma}$ is a constant vector multiplier. We, thus, introduce a constraint functional G given by

$$G = \frac{1}{8\pi^2 v^2} \int_0^1 (\rho(|\mathbf{u}|^2 - 1) + \lambda(|\mathbf{u}'|^2 - 4\pi^2 v^2) + \boldsymbol{\gamma} \cdot (\mathbf{u} \times \mathbf{u}')) dx \quad (64)$$

and consider the problem of minimizing the Lagrangian L defined by

$$\begin{aligned} L &= F - G + 2\pi^2 v^2 \\ &= \frac{1}{8\pi^2 v^2} \int_0^1 (|\mathbf{u}''|^2 - \rho(|\mathbf{u}|^2 - 1) - \lambda(|\mathbf{u}'|^2 - 4\pi^2 v^2) - \boldsymbol{\gamma} \cdot (\mathbf{u} \times \mathbf{u}')) dx \end{aligned} \quad (65)$$

subject to the antipodal junction conditions (63), which, viewed variationally, amount to antiperiodic essential boundary conditions.

3.4 Equilibrium Conditions

For a choice of \mathbf{u} satisfying (63) to deliver a local minimum of the augmented Lagrangian L defined in (65), it must satisfy the first and second variation conditions

$$\delta L = 0 \quad \text{and} \quad \delta^2 L \geq 0 \quad (66)$$

for all variations $\mathbf{v} = \delta \mathbf{u}$ admissible in the sense that they comply with the consequences

$$\mathbf{u} \cdot \mathbf{v} = 0 \quad \text{and} \quad \mathbf{u}' \cdot \mathbf{v}' = 0 \quad (67)$$

of varying the pointwise constraints (61), the consequence

$$\int_0^1 \mathbf{u}' \times \mathbf{v} \, dx = \mathbf{0} \quad (68)$$

of varying the closure condition (62), and the consequences

$$\mathbf{v}(0) = -\mathbf{v}(1), \quad \mathbf{v}'(0) = -\mathbf{v}'(1), \quad \mathbf{v}''(0) = -\mathbf{v}''(1), \quad \mathbf{v}'''(0) = -\mathbf{v}'''(1), \quad (69)$$

of varying the antipodal junction conditions (63).⁶

Varying L , integrating by parts, and using (63) and (69), we find that the first-variation condition (66)₁ takes the form

$$\int_0^1 (\mathbf{u}'''' + (\lambda \mathbf{u}')' + \boldsymbol{\gamma} \times \mathbf{u}' - \rho \mathbf{u}) \cdot \mathbf{v} \, dx = (\lambda(1) - \lambda(0)) \mathbf{u}'(0) \cdot \mathbf{v}(0). \quad (70)$$

Applying standard localization arguments, we thus obtain the Euler–Lagrange equation

$$(\mathbf{u}''' + \lambda \mathbf{u}' + \boldsymbol{\gamma} \times \mathbf{u}') = \rho \mathbf{u} \quad (71)$$

and the natural junction condition

$$\lambda(0) = \lambda(1). \quad (72)$$

Granted that (71) and (72) hold, the second variation $\delta^2 L$ of L reads

$$\delta^2 L = \int_0^1 (\mathbf{v}'''' + \lambda \mathbf{v}'' + \lambda' \mathbf{v}' + \boldsymbol{\gamma} \times \mathbf{v}' - \rho \mathbf{v}) \cdot \mathbf{v} \, dx. \quad (73)$$

Integrating by parts and invoking the admissibility conditions (69) to simplify (73), we find that the second-variation condition takes the form

$$\int_0^1 (|\mathbf{v}''|^2 - \lambda |\mathbf{v}'|^2 - \boldsymbol{\gamma} \cdot (\mathbf{v} \times \mathbf{v}') - \rho |\mathbf{v}|^2) \, dx \geq 0. \quad (74)$$

A solution $\{\mathbf{u}, \rho, \lambda, \boldsymbol{\gamma}\}$ of the boundary-value problem comprised by the Euler–Lagrange equation (71), the pointwise and global constraints (61) and (62), and the essential and natural junction conditions (63) and (72) is stable if the inequality (74) holds for all variations \mathbf{v} of \mathbf{u} that satisfy the admissibility conditions (67)–(69). With reference to (41), (56), and

⁶To obtain (68), we have used (62) and (69)₁.

(58), a Möbius band \mathcal{B} determined by any stable solution, through (60), delivers a local minimum of the bending energy E and, thus, is itself stable.

Combining the consequence $\mathbf{u} \cdot \mathbf{u}''' + 3\mathbf{u}' \cdot \mathbf{u}'' = 0$ of differentiating (61)₁ thrice with the consequence $\mathbf{u}' \cdot \mathbf{u}'' = 0$ of differentiating (61)₂, we see that \mathbf{u} must obey

$$\mathbf{u} \cdot \mathbf{u}''' = 0. \quad (75)$$

Resolving the Euler–Lagrange equation (71) in the direction of \mathbf{u} and invoking (61)₁, (61)₂, the consequence $|\mathbf{u}''|^2 + \mathbf{u}' \cdot \mathbf{u}''' = 0$ of differentiating (61)₂ twice, and (75), we obtain the identity

$$\begin{aligned} \rho &= (\mathbf{u} \cdot \mathbf{u}''' + \lambda \mathbf{u} \cdot \mathbf{u}' + \mathbf{u} \cdot (\boldsymbol{\gamma} \times \mathbf{u}))' - \mathbf{u}' \cdot (\mathbf{u}''' + \lambda \mathbf{u}' + \boldsymbol{\gamma} \times \mathbf{u}) \\ &= |\mathbf{u}''|^2 - 2\pi\nu\lambda - \boldsymbol{\gamma} \cdot (\mathbf{u} \times \mathbf{u}'). \end{aligned} \quad (76)$$

Evaluating (76) at $x = 0$ and at $x = 1$ and using the antipodal junction conditions (63)_{2,4} and the natural junction condition (72), we find that ρ must satisfy the junction condition

$$\rho(0) = \rho(1). \quad (77)$$

The boundary-value problem for $\{\mathbf{u}, \rho, \lambda, \boldsymbol{\gamma}\}$ involves one control parameter: the number ν of turns, as defined in (4), contained in a helicoidal reference configuration \mathcal{H} . Since ν does not depend on the sign of p , any solution can be used to construct an enantiomorphic pair of Möbius bands, each with the same number n of half twists.

4 Discretization

4.1 Euler–Lagrange Equation, Constraints, and Junction Conditions

To formulate a discrete version of the boundary-value problem for $\{\mathbf{u}, \rho, \lambda, \boldsymbol{\gamma}\}$, we partition the range $[0, 1]$ of the dimensionless arclength x into N subintervals of dimensionless length $h = 1/N$ and define \mathbf{u}_i , λ_i , and ρ_i , $i = 0, \dots, N$, by

$$\mathbf{u}_i = \mathbf{u}(ih), \quad \lambda_i = \lambda(ih), \quad \text{and} \quad \rho_i = \rho(ih), \quad (78)$$

where, in keeping with (63)₁, (72), and (77), the values of \mathbf{u}_i , λ_i , and ρ_i at $i = 0$ and $i = N$ must satisfy

$$\mathbf{u}_0 = -\mathbf{u}_N, \quad \lambda_0 = \lambda_N, \quad \text{and} \quad \rho_0 = \rho_N. \quad (79)$$

The discretization \mathbf{u}_i , $i = 0, \dots, N$, of \mathbf{u} can be used directly to construct a polygonal approximation of a curve on the surface of the unit sphere, namely the binormal indicatrix of \mathcal{C} . To remove the degrees-of-freedom that would otherwise arise by allowing that indicatrix to rotate rigidly about an axis through one of its points and the center of the unit sphere, it is convenient to arbitrarily choose and fix $\mathbf{u}(0) = -\mathbf{u}(1)$. With this convention, the antipodal matching condition (63)₁ and its consequence (79)₁ become moot.

We use second-order central finite differences to approximate all four derivatives of \mathbf{u} and the derivative of λ . To develop the central difference approximations that are needed to obtain discrete versions of the Euler–Lagrange equation at $i = 1$ and $i = N - 1$ and of the antipodal junction conditions (63)_{2,4}, it is therefore convenient to introduce equally spaced

ghost points, two before $i = 0$ and two after $i = N$. Recognizing from (26) and (34) that the dimensionless version \mathbf{u} of the unit binormal \mathbf{b} determines an open curve on the surface of the unit sphere, we see that \mathbf{u} has an antipodal extension \mathbf{u}^e of the form

$$\mathbf{u}^e(x) = \begin{cases} \mathbf{u}(x), & 0 \leq x \leq 1, \\ -\mathbf{u}(x-1), & 1 \leq x \leq 2. \end{cases} \quad (80)$$

With reference to (80), the values of \mathbf{u}_i at the ghost points are related to corresponding interior values through

$$\mathbf{u}_{-2} = -\mathbf{u}_{N-2}, \quad \mathbf{u}_{-1} = -\mathbf{u}_{N-1}, \quad \mathbf{u}_{N+1} = -\mathbf{u}_1, \quad \mathbf{u}_{N+2} = -\mathbf{u}_2. \quad (81)$$

For the interior points $i = 1, \dots, N-1$, the resulting discrete approximations $D_h \mathbf{u}_i$, $D_h^2 \mathbf{u}_i$, $D_h^4 \mathbf{u}_i$, and $D_h \lambda_i$ of \mathbf{u}' , \mathbf{u}'' , \mathbf{u}''' , and λ' read

$$\left. \begin{aligned} D_h \mathbf{u}_i &= \frac{\mathbf{u}_{i+1} - \mathbf{u}_{i-1}}{2h}, \quad i = 1, \dots, N-1, \\ D_h^2 \mathbf{u}_i &= \frac{\mathbf{u}_{i+1} - 2\mathbf{u}_i + \mathbf{u}_{i-1}}{h^2}, \quad i = 1, \dots, N-1, \\ D_h^4 \mathbf{u}_1 &= \frac{\mathbf{u}_3 - 4\mathbf{u}_2 + 6\mathbf{u}_1 - 4\mathbf{u}_0 - \mathbf{u}_{N-1}}{h^4}, \\ D_h^4 \mathbf{u}_i &= \frac{\mathbf{u}_{i+2} - 4\mathbf{u}_{i+1} + 6\mathbf{u}_i - 4\mathbf{u}_{i-1} + \mathbf{u}_{i-2}}{h^4}, \quad i = 2, \dots, N-2, \\ D_h^4 \mathbf{u}_{N-1} &= -\frac{\mathbf{u}_1 + 4\mathbf{u}_N - 6\mathbf{u}_{N-1} + 4\mathbf{u}_{N-2} - \mathbf{u}_{N-3}}{h^4}, \\ D_h \lambda_i &= \frac{\lambda_{i+1} - \lambda_{i-1}}{2h}, \quad i = 1, \dots, N-1. \end{aligned} \right\} \quad (82)$$

Also, as consequences of (79)₁ and (81), we see that

$$\left. \begin{aligned} D_h \mathbf{u}_0 &= \frac{\mathbf{u}_1 - \mathbf{u}_{-1}}{2h} = \frac{\mathbf{u}_1 + \mathbf{u}_{N-1}}{2h} = -D_h \mathbf{u}_N, \\ D_h^2 \mathbf{u}_0 &= \frac{\mathbf{u}_1 - 2\mathbf{u}_0 + \mathbf{u}_{-1}}{h^2} = -\frac{\mathbf{u}_{N+1} - 2\mathbf{u}_N + \mathbf{u}_{N-1}}{h^2} = -D_h^2 \mathbf{u}_N, \\ D_h^3 \mathbf{u}_0 &= -\frac{\mathbf{u}_{-2} - 2\mathbf{u}_{-1} + 2\mathbf{u}_1 - \mathbf{u}_2}{2h^3} \\ &= \frac{\mathbf{u}_{N-2} - 2\mathbf{u}_{N-1} + 2\mathbf{u}_{N+1} - \mathbf{u}_{N+2}}{2h^3} = -D_h^3 \mathbf{u}_N, \end{aligned} \right\} \quad (83)$$

from which we conclude that the discrete approximations of the antipodal conditions (63)₂₋₄ hold trivially and are of no subsequent consequence.

The discrete approximations of \mathbf{u} and \mathbf{u}' can be combined with the trapezoidal rule to approximate the integral term in (59) to yield a discretized version of the parameterization \mathbf{d} of the midline \mathcal{C} of a Möbius band \mathcal{B} , namely

$$\mathbf{d}_i = \mathbf{d}_{i-1} \pm \frac{\ell}{2\pi\nu} \begin{cases} \mathbf{u}_0 \times \mathbf{u}_{N-1}, & i = 1, \\ \mathbf{u}_i \times (\mathbf{u}_{i+1} - \mathbf{u}_{i-1}), & i = 2, \dots, N-1, \end{cases} \quad (84)$$

with $\mathbf{d}_0 = \mathbf{d}(0) = \mathbf{d}(\ell)$, where the minus and plus signs in (84) correspond to the midlines of the left- and right-handed enantiomeric Möbius bands, as obtained by substituting $p = -\ell/\nu$ and $p = \ell/\nu$ from (4) in (59), respectively. Accordingly, the discretized version of the ruled parametrization $\hat{\mathbf{y}}$ in (60) is given by

$$\mathbf{y}_i(\nu) = \hat{\mathbf{y}}(ih, \nu) = \mathbf{d}_i + \nu \mathbf{u}_i, \quad i = 0, \dots, N, \quad -a \leq \nu \leq a, \quad (85)$$

where \mathbf{d}_i is defined in (84). In view of (84) and introducing the discrete approximation

$$\mathbf{t}_i = \frac{1}{2\pi\nu} \mathbf{u}_i \times D_h \mathbf{u}_i, \quad i = 0, \dots, N, \quad (86)$$

of the unit tangent $\dot{\mathbf{d}}$ to the midline \mathcal{C} of a Möbius band \mathcal{B} , the discrete approximation of the writhe w defined in (40) is given by

$$w = \frac{1}{2\pi N^2} \left| \sum_{i=0}^{N-1} \sum_{l=0, l \neq i}^{N-1} \frac{(\mathbf{t}_i \times \mathbf{t}_l) \cdot (\mathbf{d}_i - \mathbf{d}_l)}{|\mathbf{d}_i - \mathbf{d}_l|^3} \right|. \quad (87)$$

Also, in view of (82)₂ and (83)₂, the discrete approximation of the dimensionless bending energy F defined in (58) reads

$$F = \frac{\ell}{8\pi^2 \nu^2 N} \sum_{i=0}^{N-1} |D_h^2 \mathbf{u}_i|^2 - 2\pi^2 \nu^2. \quad (88)$$

Finally, the discrete conditions arising from our finite-difference discretizations of the Euler–Lagrange equation (71), the pointwise constraints (61), and the global constraint (62) are:

- Euler–Lagrange equation (71):

$$D_h^4 \mathbf{u}_i + \lambda_i D_h^2 \mathbf{u}_i + D_h \lambda_i D_h \mathbf{u}_i + \boldsymbol{\gamma} \times D_h \mathbf{u}_i = \rho_i \mathbf{u}_i, \quad i = 1, \dots, N-1. \quad (89)$$

- Pointwise constraint (61)₁:

$$\mathbf{u}_i \cdot \mathbf{u}_i = 1, \quad i = 1, \dots, N-1. \quad (90)$$

- Pointwise constraint (61)₂:

$$\left. \begin{aligned} \mathbf{u}_1 \cdot \mathbf{u}_{N-1} &= 8\pi^2 \nu^2 h^2 - 1, \\ \mathbf{u}_{i-1} \cdot \mathbf{u}_{i+1} &= 1 - 8\pi^2 \nu^2 h^2, \quad i = 1, \dots, N-1. \end{aligned} \right\} \quad (91)$$

- Global constraint (62):⁷

$$\sum_{i=0}^{N-1} \mathbf{u}_i \times \mathbf{u}_{i+1} = \mathbf{0}. \quad (92)$$

⁷To obtain the discretized closure condition (92), we apply the trapezoidal rule of integration to (62) and invoke (83)₁ and the central difference approximation (82)₁ of \mathbf{u}' .

The system comprised by (89)–(92) consists of $5N - 1$ scalar equations for the same number of scalar unknowns $\mathbf{u}_1, \dots, \mathbf{u}_{N-1}, \lambda_1, \dots, \lambda_N, \rho_1, \dots, \rho_{N-1}$, and $\boldsymbol{\gamma}$. Granted knowledge of these quantities, λ_0 is determined from (79)₂. Also, in view of (76), the provision that \mathbf{u}_0 is given, and (83)_{1,2}, $\rho_0 = \rho_N$ is determined by

$$\rho_0 = \rho_N = |D_h^2 \mathbf{u}_0|^2 - 2\pi \nu \lambda_0 - \boldsymbol{\gamma} \cdot (\mathbf{u}_0 \times D_h \mathbf{u}_0). \quad (93)$$

4.2 Second Variation and Projected Hessian

For the previously described discretization, the second variation (74) of the dimensionless augmented Lagrangian L is approximated by the quadratic form,

$$\sum_{i=1}^{N-1} (|D_h^2 \mathbf{v}_i|^2 - \lambda_i |D_h \mathbf{v}_i|^2 - \boldsymbol{\gamma} \cdot (\mathbf{v}_i \times D_h \mathbf{v}_i) - \rho_i |\mathbf{v}_i|^2) + 2|D_h^2 \mathbf{v}_N|^2 - 2\lambda_N |D_h \mathbf{v}_N|^2, \quad (94)$$

in the admissible variations \mathbf{v}_i , $i = 0, \dots, N$. The sum (94) can be recast in matrix form $\mathbf{V}^\top \mathbf{H} \mathbf{V}$, where \mathbf{V} is the $(3N - 3) \times 1$ column matrix assembled from the admissible variations \mathbf{v}_i , $i = 1, \dots, N - 1$, and \mathbf{H} is the $(3N - 3) \times (3N - 3)$ Hessian matrix of the system (89)–(92) for determining $\mathbf{u}_1, \dots, \mathbf{u}_{N-1}, \lambda_1, \dots, \lambda_N, \rho_1, \dots, \rho_{N-1}$, and $\boldsymbol{\gamma}$. We apply the method of Nocedal and Overton [9] to derive a constraint gradient matrix \mathbf{A} and the associated projected Hessian $\hat{\mathbf{H}}$. A constraint gradient matrix \mathbf{A} of dimension $(2N + 2) \times (3N - 3)$ can be obtained by differentiating the $2N + 2$ scalar constraints comprised by the $N - 1$ scalar constraints in (90), the N constraints in (91), and the three scalar constraints in (92) with respect to $3N - 3$ unknowns \mathbf{u}_i , $i = 1, \dots, N - 1$. Because the $3N - 3$ scalar unknowns \mathbf{u}_i , $i = 1, \dots, N - 1$, must satisfy $2N + 2$ constraints, there are a total of $(3N - 3) - (2N + 2) = N - 4$ independent scalar unknowns. The matrix \mathbf{Z} of dimension $(3N - 3) \times (N - 4)$, which can be derived from the QR factorization of \mathbf{A} , consists of orthonormal columns that span the null space of the transpose \mathbf{A}^\top of \mathbf{A} . The $(N - 4) \times (N - 4)$ projected Hessian $\hat{\mathbf{H}}$ matrix is then given by $\hat{\mathbf{H}} = \mathbf{Z}^\top \mathbf{H} \mathbf{Z}$. If each eigenvalue of $\hat{\mathbf{H}}$ evaluated at an equilibrium solution is positive, then that equilibrium solution is stable. If, otherwise, one or more eigenvalues of $\hat{\mathbf{H}}$ is negative or zero, then that equilibrium solution corresponds to a saddle point.

5 Numerical Results

Using the *Levenberg–Marquardt Algorithm* from the *fsolve* package of MATLAB to solve the system (89)–(92) of $5N - 1$ nonlinear equations, we found that the choice $N = 150$ was sufficient to accurately resolve each solution obtained to a tolerance of 10^{-8} . To assess the stability of each numerical solution to the equilibrium conditions, we used the *eig* package of MATLAB to compute the $N - 4$ eigenvalues of the projected Hessian $\hat{\mathbf{H}}$ derived from the quadratic form (94).

Given a vector $\boldsymbol{\omega}$ and the corresponding rotation $\boldsymbol{Q} = \exp(\boldsymbol{\omega} \times)$, it is evident that the Lagrangian L defined in (65) is invariant under transformations of the form $\{\mathbf{u}, \boldsymbol{\gamma}\} \mapsto \{\boldsymbol{Q}\mathbf{u}, \boldsymbol{Q}\boldsymbol{\gamma}\}$.⁸ Consistent with this observation, we found that $\hat{\mathbf{H}}$ has three degenerate eigenvalues due to the rigid mode corresponding to the additional degree-of-freedom $\boldsymbol{\omega}$ that are not germane to the stability of our solutions. We therefore assessed stability by determining

⁸Here, $\boldsymbol{\omega} \times$ is the unique skew tensor with axial vector $\boldsymbol{\omega}$; see Bauchau and Trainelli [10] for further detail.

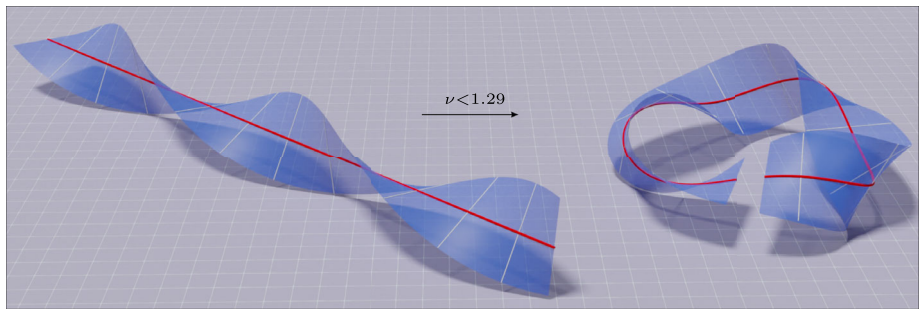


Fig. 4 The closure constraint cannot be met when attempting to bend a helicoidal reference configuration \mathcal{H} with $\nu < 1.29$ turns into a Möbius band \mathcal{B} . To construct the graphs in this figure, ν was taken to equal 1.25

the sign of the smallest nonvanishing eigenvalue of $\hat{\mathbf{H}}$. Although stable and saddle solutions were found, we focus subsequently on stable solutions.

We first tried to solve (89)–(92) for the conservative choice $\nu = 10^{-2}$. After failing in that effort, we systematically increased ν by increments of 10^{-2} until finding a first stable solution at $\nu = 1.29$. The existence of a threshold below which no stable solution exists is consistent with the intuitive expectation that it should not be possible to connect the ends of a helicoidal reference configuration \mathcal{H} with ν turns to form a Möbius band \mathcal{B} unless ν is sufficiently large. It is impossible to meet the closure condition (33) for $\nu < 1.29$, as illustrated in Fig. 4.

Further increasing ν by increments of 10^{-2} , we found a stable solution for $1.30 \leq \nu \leq 1.39$ and discovered a second threshold, at $\nu = 1.40$, at and above which we found two stable solutions. Above $\nu = 13.5$, we stopped systematically increasing ν by increments of 10^{-2} in favor of testing only select values of ν . Although only two stable solutions were found for each $\nu > 1.40$ that we considered, we cannot rule out the existence of additional thresholds beyond which more than two stable solutions exist.

Since ν , as defined by (4), is independent of the sign of the pitch p of a helicoidal reference configuration \mathcal{H} , any solution corresponding to a given value of ν can be used to construct an enantiomorphic pair of Möbius bands, each with the same number n of half twists. From this juncture onward, without loss of generality, we use the version of (84) with a plus sign in junction with (85) to construct and graph only the right-handed stable Möbius band \mathcal{B} determined by each stable solution obtained for $1.29 \leq \nu \leq 13.5$. Inspecting the graphs visually, we found that each stable Möbius band is an unknot.⁹ After computing the discrete approximation (87) of the writhe w of the midline \mathcal{C} of each stable Möbius band \mathcal{B} , we evaluated (39) to compute the number n of half twists in each such \mathcal{B} . In so doing, we found that n increases stepwise in accord with $n = 2j + 1$, $j = 1, \dots, 13$, as ν increases from $\nu = 1.29$ to $\nu = 13.5$. In so doing, we also confirmed the accuracy of (39)–(40), using (87) to approximate w , by visual inspection of the graphs. We consistently found that one of the two stable Möbius bands determined for each $\nu \geq 1.40$ has an additional full twist and larger dimensionless bending energy than the other.

The lower envelope of the dimensionless bending energy F determined by evaluating (88) at each stable solution obtained for $1.29 \leq \nu \leq 13.5$ is shown in Fig. 5. The values of ν corresponding to the peaks and valleys of that envelope are especially significant. Machine precision estimates of those values, obtained by the interval halving method, are listed in

⁹In contrast, we found that Möbius bands determined by saddle solutions can be unknotted or knotted.

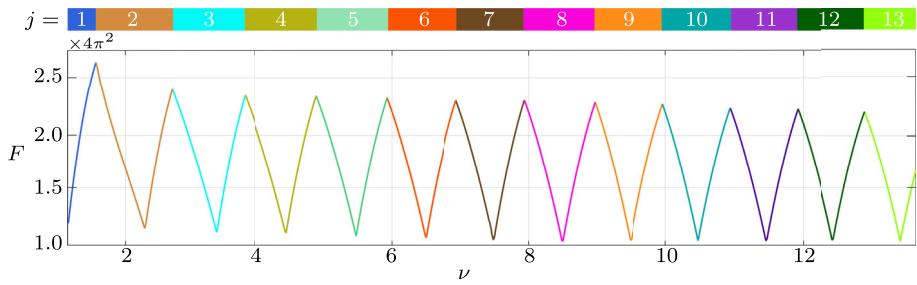


Fig. 5 Plot of the lower envelope of the dimensionless bending energy F of each stable Möbius band obtained by an isometric, chirality preserving deformation of a helicoidal reference configuration \mathcal{H} with $1.29 \leq \nu \leq 13.5$ turns. The colors on the envelope represent the number $n = 2j + 1$, $j = 1, \dots, 13$, of half twists of the Möbius band obtained for each value of j , as indicated by the color panel above the plot

Table 1 Number $\bar{\nu}_j$ of turns and dimensionless bending energy \bar{F}_j at the j -th peak, $j = 1, \dots, 12$, of the lower envelope shown in Fig. 5

j	$\bar{\nu}_j$	\bar{F}_j
1	1.76661986	106.253778
2	2.80112699	95.1966624
3	3.85154962	93.6299380
4	4.87014125	92.7106101
5	5.90464838	91.9797528
6	6.89140903	91.4205339
7	7.89408517	90.6557287
8	8.89676131	89.9428874
9	9.86760647	89.1795797
10	10.8384516	88.3258574
11	11.8411277	87.3673587
12	12.8060574	86.3857150

Tables 1 and 2. For convenience, we denote the values of ν and F at the j -th valley by ν_j and F_j , $j = 1, \dots, 13$. Similarly, we denote the values of ν and F at the j -th peak by $\bar{\nu}_j$ and \bar{F}_j , $j = 1, \dots, 12$.

With reference to Fig. 5, we observe that:

- Each stable solution obtained for $\nu_1 \leq \nu \leq \bar{\nu}_1$ determines a stable Möbius band \mathcal{B} with $n = 3$ half twists.
- For $j = 1, \dots, 11$, each stable solution obtained for $\bar{\nu}_j < \nu < \bar{\nu}_{j+1}$ determines a stable Möbius band \mathcal{B} with $n = 2j + 3$ half twists.
- For $\bar{\nu}_{12} < \nu \leq 13.5$, each stable solution determines a stable Möbius band \mathcal{B} with $n = 27$ half twists.

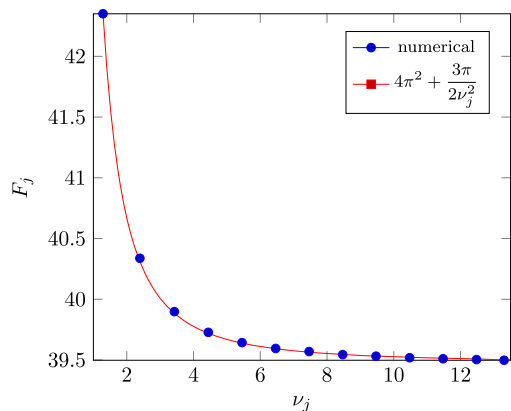
Letting \mathcal{B}_j denote the stable Möbius band with $n = 2j + 1$ half twists determined by any stable solution obtained for ν_j , $j = 1, \dots, 13$, we also notice from Fig. 5 that:

- For $j = 1, \dots, 13$, \mathcal{B}_j has lower dimensionless bending energy than every other stable Möbius band \mathcal{B} with $n = 2j + 1$ half twists and is, thus, energetically optimal.

Table 2 Number ν_j of turns, dimensionless bending energy F_j , and number $n = 2j + 1$ of half twists at the j -th valley, $j = 1, \dots, 13$, of the lower envelope shown in Fig. 5

j	ν_j	F_j	n
1	1.28811996	42.3505578	3
2	2.37322017	40.3373757	5
3	3.41108030	39.8980017	7
4	4.43119251	39.7274045	9
5	5.44384690	39.6429593	11
6	6.45608744	39.5947565	13
7	7.46346708	39.5693952	15
8	8.47030065	39.5440338	17
9	9.46821609	39.5313042	19
10	10.4758892	39.5185746	21
11	11.4779164	39.5101139	23
12	12.4795931	39.5033033	25
13	13.4809940	39.5013649	27

Fig. 6 Plot of the dimensionless bending energy F_j of each energetically optimal band \mathcal{B}_j versus the number ν_j of turns in its referential precursor obtained for $j = 1, \dots, 13$. The numerical values of ν_j and F_j , $j = 1, \dots, 13$, are provided in Table 2



- For $j = 1, \dots, 13$, the dimensionless bending energy F_j of \mathcal{B}_j decreases monotonically as j increases from $j = 1$ to $j = 13$.¹⁰

In connection with the last of the above points, we see from a plot of F_j versus ν_j shown in Fig. 6 that, for $j = 1, \dots, 13$, F_j decays in accord with the heuristic relation

$$F_j \approx 4\pi^2 + \frac{3\pi}{2\nu_j^2}. \quad (95)$$

From plan and isometric views of \mathcal{B}_j , $j = 1, \dots, 12$, provided in Figs. 7 and 8, we gain the impression that the energetically optimal Möbius band \mathcal{B}_j with $n = 2j + 1$ half twists exhibits $(2j + 1)$ -fold rotational symmetry. This impression is confirmed by plots presented in Fig. 9, from which it is evident that the discrete approximation (86) of the unit tangent \vec{d} to the midline \mathcal{C}_j of each \mathcal{B}_j with $n = 2j + 1$ half twists that is depicted in Figs. 7 and 8 is periodic with period $1/n$. For $j = 1, \dots, 13$, all stable Möbius bands with $n = 2j + 1$

¹⁰There is a 17.9% difference between F_1 and F_{13} .



Fig. 7 Plan views of each energetically optimal Möbius band \mathcal{B}_j with $n = 2j + 1$ half twists obtained for each value v_j , $j = 1, \dots, 12$, of v listed in Table 2. The helicoidal precursor of each Möbius band depicted here has length-to-radius aspect ratio $\ell/a = 40$. Since \mathcal{B}_j has $2j + 1$ rulings perpendicular to its plan view, the images above may convey the impression that the rulings of \mathcal{B}_j are discontinuous at $2j + 1$ points and, thus, that the width of \mathcal{B}_j vanishes at those points. Any such impression is illusory

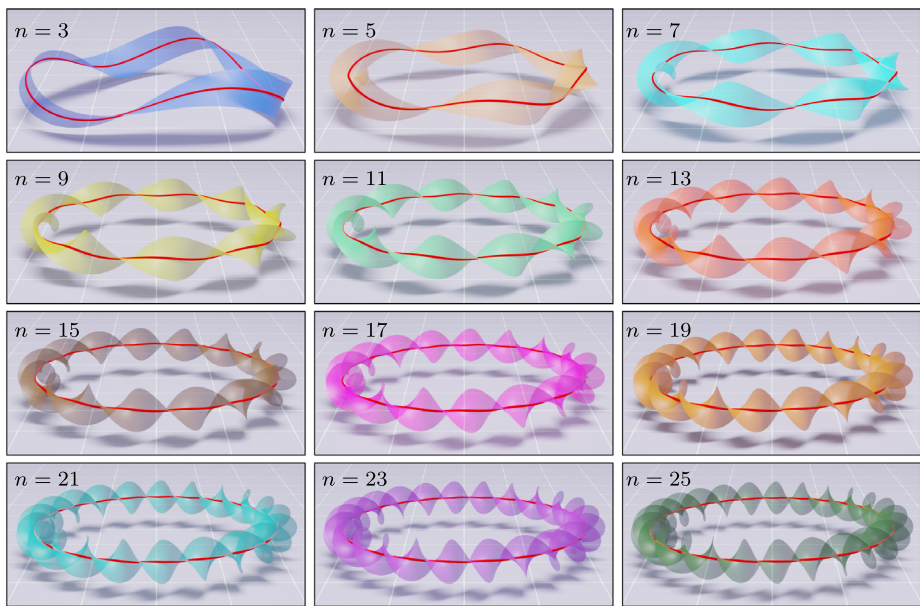


Fig. 8 Isometric views of each energetically optimal Möbius band \mathcal{B}_j with $n = 2j + 1$ half twists obtained for each value v_j , $j = 1, \dots, 12$, of v listed in Table 2. The helicoidal precursor of each Möbius band depicted here has length-to-radius aspect ratio $\ell/a = 40$

half twists except the energetically optimal Möbius band \mathcal{B}_j exhibit broken symmetry. This finding is illustrated in Fig. 10, where we graph the energetically optimal Möbius band \mathcal{B}_2 with $n = 5$ half twists and two stable Möbius bands with the same number of half twists, and equal dimensionless bending energy $F = 50.0 > F_2 = 40.3$, obtained for $v = 2.26$ and $v = 2.45$.

The machine precision estimates of v_j , $j = 1, \dots, 13$, listed in Table 2 were obtained by solving (89)–(92) for $v = 1.29 + 10^{-2}m$, $m = 0, 1, \dots, 1221$, extracting lower precision estimates of v_j from a rough version the lower envelope shown in Fig. 5, and, finally, applying the interval-halving method to obtain refined estimates. We next develop a heuristic relation between v_j and j which allows us to avoid this computationally costly procedure. For an energetically optimal Möbius band \mathcal{B}_j with $n = 2j + 1$ half twists, we see from (39) that v_j is given by

$$v_j = \frac{2j + 1}{2} - w_j, \quad (96)$$

where w_j is the writhe of the midline C_j of \mathcal{B}_j . To obtain a provisional relation between w_j and j , we use (87) to compute w_j for $j = 1, \dots, 13$. From the plot provided in Fig. 11, we infer that w_j is closely approximated by the heuristic relation

$$w_j \approx \frac{2}{\pi(2j + 1)}, \quad j = 1, \dots, 13. \quad (97)$$

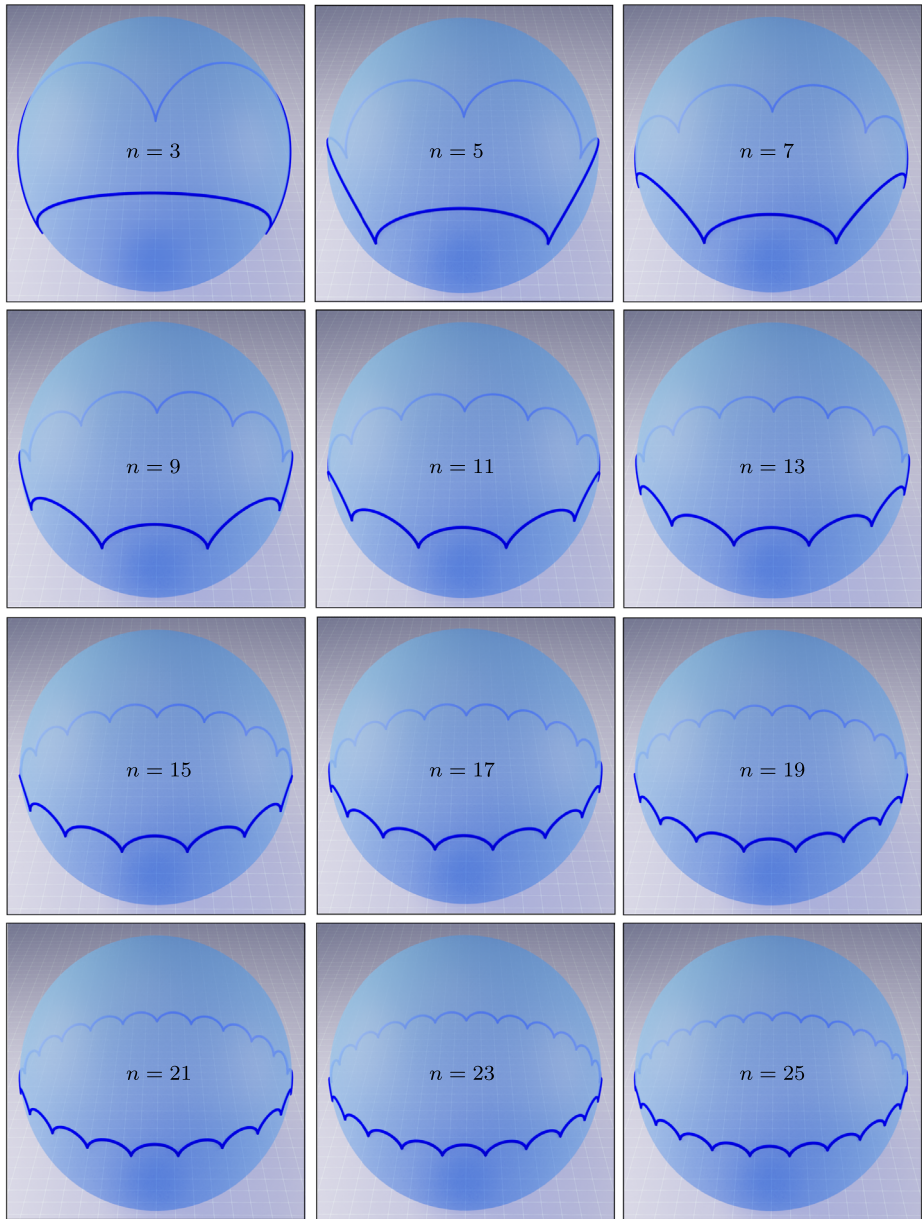


Fig. 9 Tangent indicatrix of the midline of each energetically optimal Möbius band \mathcal{B}_j with $n = 2j + 1$ half twists, $j = 1, \dots, 12$, shown in Figs. 7 and 8

From Table 3, we see that, for $j = 1, \dots, 13$, the values of v_j^* determined by

$$v_j^* = \frac{2j+1}{2} - \frac{2}{\pi(2j+1)} \quad (98)$$

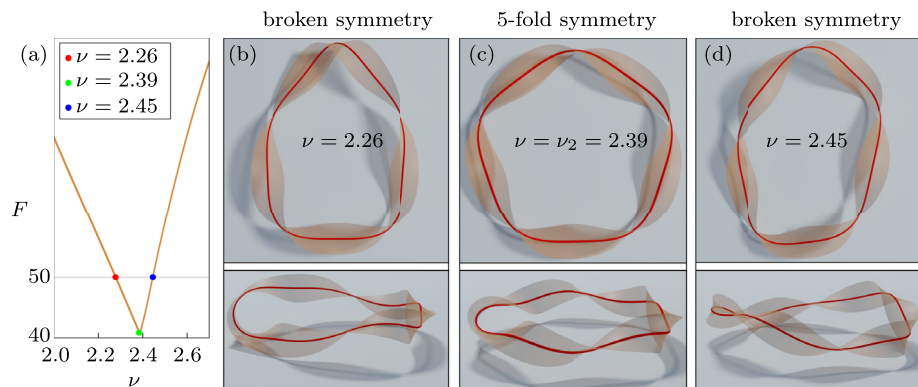
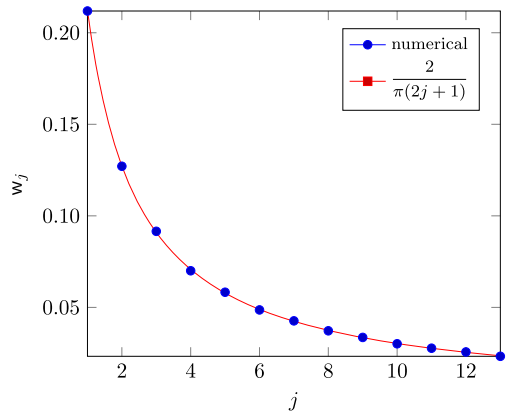


Fig. 10 (a) Zoomed-in view of an interval about the valley point $\nu_2 = 2.39$ of the lower envelope shown in Fig. 5. The green dot marks the value F_2 of the dimensionless bending energy F of the energetically optimal Möbius band B_2 with $n = 5$ half twists and 5-fold rotational symmetry. The red and blue dots mark the shared value of the dimensionless bending energy $F > F_2$, at $\nu = 2.26$ and $\nu = 2.45$, of stable Möbius bands which also have $n = 5$ half twists but broken symmetry. Plan and isometric views of the Möbius bands obtained for $\nu = 2.26$, $\nu = \nu_2 = 2.39$, and $\nu = 2.45$ appear in (b), (c), and (d), respectively

Fig. 11 Plots of the heuristic relation (97) for the writhe w_j of the midline C_j of each energetically optimal Möbius band B_j with $n = 2j + 1$ half twists versus j for $j = 1, \dots, 13$



differ from the machine precision values of ν_j in Table 2 by at most 0.091%.

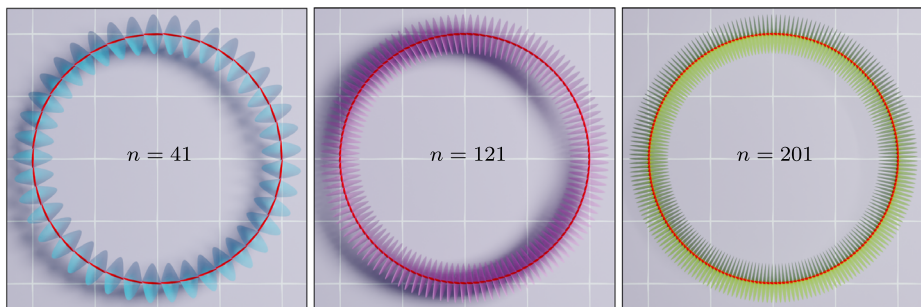
To test whether (98) can be used to provide an accurate initial guess for values of ν_j with $j > 13$, we solved (89)–(92) in an interval about $\nu = \nu_j^*$ for $j = 10q$, $q = 2, 3, \dots, 10$, and used interval halving to obtain machine precision estimates of ν_j . From Table 4, we see that, for the choices of j considered, the values of ν_j^* and the refined values of ν_j differ by at most 0.067%. Consistent with our results for ν_j , $j = 1, \dots, 13$, we found that the energetically optimal Möbius band B_j determined by each value of ν_j in Table 4 has $n = 2j + 1$ half twists and has $(2j + 1)$ -fold rotational symmetry. This finding is illustrated in Figs. 12 and 13, where we present plan and isometric views of B_j for $j = 20$, $j = 60$, and $j = 100$, and in Fig. 14, where we plot the corresponding tangent indicatrices. From plots shown in Fig. 15 of the empirical relation (95) for the dimensionless bending energy F_j and the numerically values of F_j obtained for each considered choice of j , we see that (95) remains accurate up to $j = 100$. This boosts our confidence in the heuristic foundation of the expression (98) for the approximation ν_j^* of ν_j .

Table 3 Values of v_j^* , v_j , and percent difference for $j = 1, 2, \dots, 13$

j	v_j^*	v_j	% difference
1	1.28779341	1.28811996	0.01267706
2	2.37267605	2.37322017	0.01465063
3	3.40905432	3.41108030	0.02970587
4	4.42926447	4.43119251	0.02176005
5	5.44212548	5.44384690	0.01581320
6	6.45102925	6.45608744	0.03918916
7	7.45755868	7.46346708	0.03959781
8	8.46255178	8.47030065	0.04576234
9	9.46649370	9.46821609	0.09096469
1	10.4696848	10.4758892	0.02962153
11	11.4723209	11.4779164	0.02438101
12	12.4745352	12.4795931	0.02026879
13	13.4764215	13.4809940	0.01696194

Table 4 Values of v_j^* , v_j , and percent difference for $j = 10q$, $q = 2, 3, \dots, 10$

j	v_j^*	v_j	% difference
20	20.4844727	20.4862279	0.00428404
30	30.4895636	30.4866293	0.00481221
40	40.4921405	40.4665585	0.03159883
50	50.4936968	50.4611965	0.03219293
60	60.4947387	60.4376458	0.04721057
70	70.4954850	70.4043185	0.06470311
80	80.4960458	80.4016244	0.05868412
90	90.4964828	90.3977727	0.05456786
100	100.496833	100.361300	0.06747688

**Fig. 12** Plan views of each energetically optimal Möbius band \mathcal{B}_j with $n = 2j + 1$ half twists, for $j = 20$, $j = 60$, and $j = 100$

We found that the midline \mathcal{C}_j of an energetically optimal Möbius band \mathcal{B}_j with $n = 2j + 1$ half twists becomes increasingly planar as j increases. This phenomenon is illustrated in Fig. 16, which contains plots the deviation Δ_j of \mathcal{C}_j from its plane of symmetry and graphs

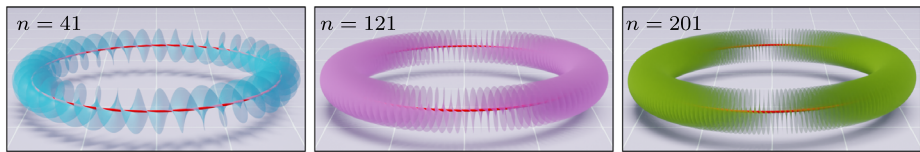


Fig. 13 Isometric views of each energetically optimal Möbius band \mathcal{B}_j with $n = 2j + 1$ half twists, for $j = 20$, $j = 60$, and $j = 100$

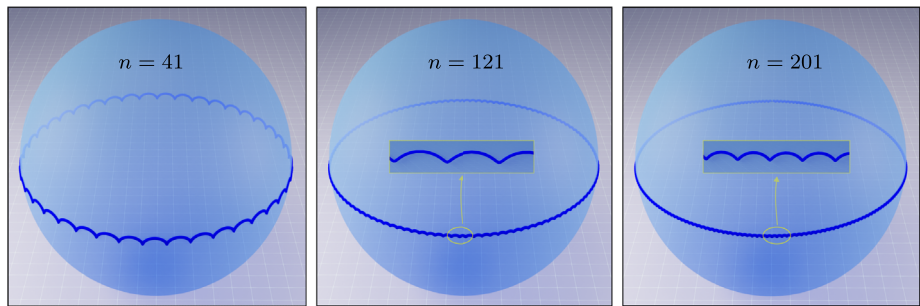
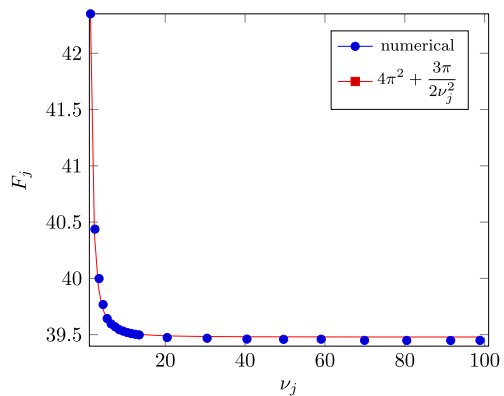


Fig. 14 Tangent indicatrix of the midline of each energetically optimal Möbius band \mathcal{B}_j with $n = 2j + 1$ half twists, for $j = 20$, $j = 60$, and $j = 100$. From zoomed-in views contained in bounding boxes with identical dimensions, it is evident that the amplitude of undulation decreases and the number of undulations increases as $n = 2j + 1$ increases

Fig. 15 Plot of the dimensionless bending energy F_j of each energetically optimal Möbius band \mathcal{B}_j versus ν_j for all values of ν_j listed in Tables 3 and 4



of those midlines for $j = 1, 2, 3, 9$, and $j = 100$, and in Fig. 17, where plot of the natural logarithm of the maximum value Δ_j^{\max} of Δ_j versus the natural logarithm $2j + 1$ for $j = 1, 2, \dots, 13$, and $j = 10q$, $q = 2, 3, \dots, 10$. From Fig. 16, it is evident that Δ_j has period $1/n$ and its amplitude decreases with n . From Fig. 17, we see that Δ_j^{\max} obeys a scaling relation of the form

$$\Delta_j^{\max} \sim \frac{1}{(2j + 1)^2}. \quad (99)$$

Thus, $\Delta_j \rightarrow 0$ as $j \rightarrow \infty$. The midline C_j of \mathcal{B}_j with $n = 2j + 1$ half twists undulates $2n$ times about its plane of symmetry. If the length ℓ of C_j is fixed, then the amplitude of the

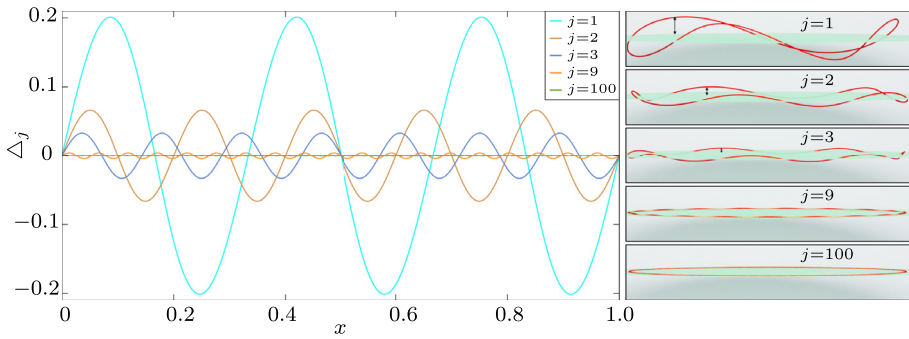
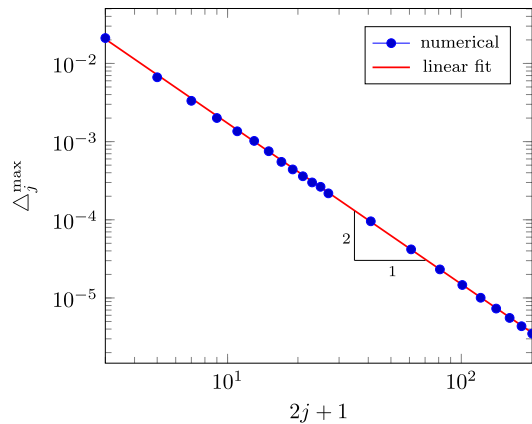


Fig. 16 Left: Plots of the deviation Δ_j of the midline C_j of an energetically optimal Möbius band B_j with $n = 2j + 1$ half twists from its plane of symmetry versus the dimensionless arclength x for representative values 1, 2, 3, 9, and 100 of j . Right: Graphs of the midline C_j of B_j as $j = 1, 2, 3, 9$ and $j = 100$

Fig. 17 Log-log plot of the maximum dimensionless deviation Δ_j^{\max} of the midline C_j of an energetically optimal Möbius band B_j with $n = 2j + 1$ half twists from its plane of symmetry versus the $n = 2j + 1$



undulation must decrease as j increases. That C_j becomes increasingly planar as j increases is therefore consistent with intuition. However, with reference to (23), the midline C_j of B_j cannot be planar since it must have uniform torsion

$$\tau_j = \frac{2\pi v_j}{\ell}. \quad (100)$$

Using (98) in (100), we see that

$$\tau_j \approx \frac{\pi(2j+1)}{\ell} - \frac{4}{(2j+1)\ell} \quad (101)$$

and, thus, that τ_j increases monotonically with the number $2j + 1$ of turns in B_j .

A solution to (89)–(92) obtained for a choice of $v \geq 1.29$ can be used to construct enantiomeric Möbius bands corresponding to enantiomeric helicoidal reference configurations of axial length ℓ with $v \geq 1.29$ turns. While the right-handed Möbius band is determined by (85) after using the solution obtained for the given choice of v to construct d_i , $i = 1, \dots, N$, by choosing the plus sign in (84), its left-handed enantiomer is determined in the same way except that the minus sign is chosen in (84). It is evident from (88) that the enantiomeric

Möbius bands determined for a given choice of $\nu \geq 1.29$ have identical dimensionless bending energy. Our results concerning energy minima, therefore, apply equally well to left-handed Möbius bands. Graphs of the left-handed counterparts of the energetically optimal Möbius bands presented in this section are provided in our Supplemental Material. Whereas the right-handed Möbius band determined for each ν arises from isometrically deforming a right-handed helicoidal reference configuration with axis of length ℓ and positive pitch $p = \ell/\nu$, the left-handed enantiomer of that Möbius band arises from isometrically deforming a left-handed helicoidal reference configuration with axis of length ℓ and negative pitch $p = -\ell/\nu$.

6 Summary and Discussion

We derived the exact provisions under which a (circular) helicoidal reference configuration \mathcal{H} of given pitch $p \neq 0$, axial length ℓ , and radius a can be isometrically deformed into a ruled Möbius band \mathcal{B} with the same chirality as \mathcal{H} . Leveraging those provisions, we found that the rulings of any such \mathcal{B} must align with the unit binormal \mathbf{b} of the midline \mathcal{C} of \mathcal{B} and, moreover, that \mathcal{C} must be a geodesic of \mathcal{B} and must have uniform torsion $\tau = 2\pi/p$. On this basis, we obtained a general representation for \mathcal{B} in terms of \mathbf{b} , with parametric dependence on p and ℓ . Granted that the energy, per unit area, stored in bending \mathcal{H} to \mathcal{B} is of the form $2\mu H^2$, with H being the mean curvature of \mathcal{B} , we discovered that the total bending energy E reduces, without approximation and in closed form, and valid independent of the width of \mathcal{B} , to an integral over \mathcal{C} , with integrand proportional to the square of the normal curvature k of \mathcal{C} . We then formulated a variational problem for determining \mathbf{b} subject to constraints needed to ensure that the deformation η from \mathcal{H} to \mathcal{B} is isometric and that the ends of \mathcal{H} join smoothly to form \mathcal{B} . We found that the dimensionless version of our variational problem involves only one input parameter: $\nu = \ell/|p|$, which measures the number of times \mathcal{H} turns around its axis. Deriving the first and second variation conditions for our dimensionless variational problem, we developed a numerical method for satisfying those conditions. Using that method, we constructed solutions corresponding to local minima of the dimensionless bending energy F . We solved that problem exhaustively for values of ν up to 13.5 and then selectively for values of ν up to slightly above 100. Over the considered range of ν , we found that any \mathcal{B} determined by such a local minimum of F is unknotted and has an odd number n of half twists between $n = 3$ and $n = 201$. For $n = 2j + 1$, $j = 1, \dots, 13$, we found that there is a choice ν_j of ν such that the corresponding Möbius band \mathcal{B}_j exhibits n -fold rotational symmetry and has lower dimensionless bending energy than any other stable Möbius band \mathcal{B} with the same number of half twists. For select values of j between $j = 14$ and $j = 100$, we found that a heuristic approximation ν_j^* of ν_j obtained by post-processing our numerical results for $j = 1, \dots, 13$ can be used reliably to compute a solution that determines an energetically optimal Möbius band \mathcal{B}_j with $n = 2j + 1$ half twists and n -fold rotational symmetry. We therefore infer that a helicoid \mathcal{H} cannot be isometrically deformed into a ruled Möbius band \mathcal{B} with n half twists and n fold rotational symmetry unless it has the specific number ν of turns needed to ensure that \mathcal{B} is energetically optimal. These energetically optimal Möbius bands emerge naturally by minimizing F without imposing symmetry requirements of any kind.

The absence of a solution to our variational problem for $\nu < 1.29$ is analogous to a discovery of Schönke and Fried [11], who found that a chain made from $N \geq 7$ identical twisted links connected by hinges cannot be closed into a linkage with the topology of a Möbius band unless the twist angle exceeds a certain critical threshold that depends on N .

Each linkage consisting of $N \geq 7$ critically twisted links of length ℓ/N can be thought of as a discrete approximation of the Möbius band we obtain for $\nu = \nu_1 = 1.29$. Moreover, the relaxed configuration of the open chain that forms any such linkage is a discrete approximation of a helicoid. Passing to the limit $N \rightarrow \infty$ with ℓ fixed, Schönke and Fried [11] found that the sequence of critically twisted linkages converges to a Möbius band with $n = 3$ half twists and 3-fold rotational symmetry. That limit surface is a binormal scroll and its midline is a geodesic which has uniform torsion equal to the value $\tau_1 = 2\pi\nu_1/\ell$ of the torsion of the midline of the Möbius band \mathcal{B}_1 with $n = 3$ half twists obtained in the present work. Thus, that limit surface is identical to \mathcal{B}_1 .

For $1.29 \leq \nu \leq 13.5$, we discovered two branches of solutions that minimize F . The lower envelope of F versus ν , shown in Fig. 5, was constructed from those branches. Although we did not encounter evidence of more than two solution branches for $1.29 \leq \nu \leq 1.01 \times 10^2$, we cannot dismiss their possible existence. We speculate, however, that for any additional solution that might exist for a choice of ν considered in the present work would have dimensionless bending energy greater than the corresponding values of F on the branches of solutions discussed here.

For certain values of ν , we obtained solutions that yield knotted Möbius bands. However, each such solution was found to be a saddle point of the dimensionless bending energy F . Langer and Singer [12] conjectured that a knotted elastica cannot be in equilibrium unless it has points of self-contact. Since the integrand of the dimensionless bending energy F is proportional to the square of the normal curvature k of the midline \mathcal{C} of \mathcal{B} and since each knotted \mathcal{B} we encountered was observed to be free of self-contact, our findings concerning the stability of knotted Möbius bands appear to support this conjecture.

We also obtained saddle solutions that yield unknotted Möbius bands which might serve to model transition states in biological processes. Louie and Somorjai [13] observed that β -barrel proteins with antiparallel strands constructed from α -helical proteins, which resemble the midlines of the Möbius bands corresponding to our unknotted saddle solutions, are intermediate states in this protein folding transformation. Stępień et al. [14] observed that porphyrins, which exhibit configurations that are also similar to the Möbius bands corresponding to our unknotted saddle solutions, might be stabilized by electronic interactions. Wallin et al. [15] found that attractive non-native interactions are vital for forming knotted proteins. Liu et al. [16] discovered that knotted DNA rings transform into circular rings in solutions of sufficiently low ion concentrations, indicating that ionic interactions might stabilize knots. Based on these studies and our findings, we suspect that bending energy is insufficient to stabilize the saddle solutions and that this deficiency might be rectified by including energetic contributions that account for electrostatic and short-range weak interactions.

A unit binormal \mathbf{b} determined by solving our variational problem can be used to construct a Möbius band \mathcal{B} of width equal to twice the radius a of its helicoidal precursor \mathcal{H} . However, \mathcal{B} will intersect itself if a is too large. It would be cumbersome to use our numerical method to determine the supremum of a below which a helicoidal reference configuration \mathcal{H} with ν turns can be deformed isometrically into a Möbius band \mathcal{B} which does not intersect itself. A more effective approach to the challenge might rest on augmenting our framework to include a constraint that forbids the interpenetration of matter.

Our framework provides a foundation for exploring analogous deformations of other reference shapes, including hyperbolic paraboloids of one sheet, which, as Lasters et al. [17] observe, resemble protein β -barrels. Any ruled surface can sustain an isometric deformation if the rulings are rigid material line elements. Classifying the stable deformed configurations of all such reference shapes might facilitate studies of molecular synthesis and protein

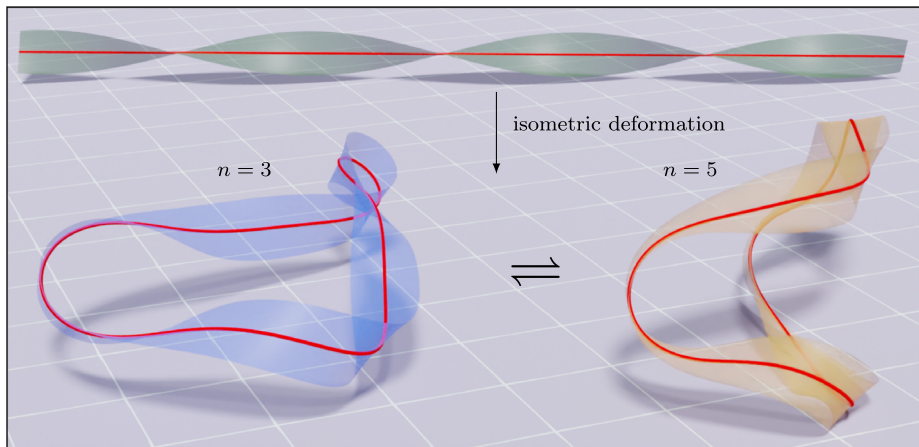


Fig. 18 Topological switch between stable Möbius bands constructed from isometric deformations of a reference helicoid \mathcal{H} with $\nu = \bar{\nu}_1 = 1.77$ turns, both corresponding to the first peak of the lower envelope shown in Fig. 5. Although the Möbius bands on the left and the right have $n = 3$ and $n = 5$ half twists, respectively, they have the same dimensionless bending energy $\bar{F}_1 = 1.06 \times 10^2$

folding, helping to eliminate backbone strain of the kind discussed by Dou et al. [18]. Our findings might provide guidelines for designing novel deployable structures such as those described by Schönke and Fried [11, Figs. 7–8]. Since reported configurations allow elastic bending, they can further be used in compliant mechanisms. Modularly using connected Möbius bands in lattices could lead to bi- or multi-stable systems. The analogy between bendable Möbius bands and linkages with torsional spring hinges poses various vital questions regarding the constructability and stability of the resulting mechanisms.

Wang et al. [19] devised a strategy for synthesizing Möbius molecules that can switch between distinct topologies. Our framework could provide guidelines for making uniformly twisted, adjustable, and topologically switchable molecules. For the value $\bar{\nu}_j$, $j = 1, 2, \dots, 12$, of ν corresponding to each peak of the lower envelope shown in Fig. 5, two co-existing equilibrated Möbius bands have identical dimensionless bending energy $F = \bar{F}_j$ but different numbers, $n = 2j + 1$ and $n = 2j + 3$, of half twists. Since those Möbius bands can both be constructed from a reference helicoid with $\nu = \bar{\nu}_j$ turns, machine precision values of which are given in Table 1, a topological switch between them is feasible, entirely without stretching. An example of such a switch is illustrated, for the case $j = 1$ involving Möbius bands with $n = 3$ and $n = 5$ half twists, in Fig. 18. Converting one of these Möbius bands into the other would necessarily require the ability to (i) cut a Möbius band along one of its rulings, (ii) increase or reduce the number of twists of an open ribbon by one full twist while ensuring that chirality is preserved, and (iii) reconnect the ends of the open ribbon obtained after altering its number of twists. Each stable Möbius band obtained in this work is a static equilibrium configuration corresponding to a local minimizer of the underlying bending energy. A dynamical theory that could describe the folding pathway traversed when bending a reference helicoid into a Möbius band or the switching pathways between two coexisting Möbius bands with distinct numbers of half twists might be a worthwhile direction for future research.

Synthesizing a Möbius molecule with a chosen chirality is known to be challenging. Batch processes designed to produce chiral molecules often yield mixtures in which right- and left-handed molecules are present. Han et al. [20] synthesized Möbius molecules by

folding and cutting DNA and observed nearly 1:1.4 distribution of left and right-handed Möbius molecules. In an effort to produce self-assembled molecules of a chosen chirality, Geng et al. [21] used chiral block copolymers as reference molecules. Their process predominantly yielded Möbius bands with left-handed chirality. By bending and cyclizing twisted fibers resembling circular helicoids, Ouyang et al. [22] found that right- and left-handed fibers exclusively yielded right- and left-handed Möbius molecules, respectively. Ouyang et al. [22] also acknowledged the challenges entailed in fabricating twisted fibers that yield self-assembled Möbius bands with targeted numbers of half twists. Our chirality preserving isometric deformations might provide a basis for developing alternative strategies for synthesizing Möbius molecules with desired chirality. Moreover, our numerical results might help design reference molecules that could be self-assembled into Möbius molecules with programmed numbers of half twists.

Naturally occurring and synthetic Möbius bands that resemble the energetically optimal Möbius bands obtained here have many potential applications. Rosengren et al. [23] demonstrated that Möbius cyclotides are very resistant to proteolysis, which makes them excellent templates for drug design applications, as revealed by Craik et al. [24], and insecticidal agents, as shown by Jennings et al. [25]. Irobalieva et al. [26] showed that supercoiled DNA plasmids adopt diverse three-dimensional conformations ranging from circular to lemniscular. These configurations are crucial for DNA functionalities and are similar to our energetically optimal Möbius bands shown in Fig. 7. In a review of the structural design and self-assembly of DNA origami, Hong et al. [27] highlighted the utility of synthetic DNA plasmids, resembling our Möbius bands, in applications such as in electronics, elaborated by Maune et al. [28] and in drug delivery, as discussed by Zhang et al. [29]. We anticipate our work will provide new pathways for constructing synthetic molecules, thereby hastening advances in the above applications. In particular, our heuristic relation between the number $n = 2j + 1$ of half twists in an energetically optimal Möbius band \mathcal{B}_j and the number ν_j of turns of its helicoidal precursor \mathcal{H} establishes a guideline for selecting a reference helicoid that can be used to synthesize a stable Möbius band with n -fold rotational symmetry.

Appendix A

A.1 Metric Coefficients

The metric coefficients of a helicoidal reference configuration \mathcal{H} with parameterization $\hat{\mathbf{x}}$ of the form (1)–(2) are given by

$$\left. \begin{aligned} \hat{\mathbf{x}}_s(s, v) \cdot \hat{\mathbf{x}}_s(s, v) &= 1 + \frac{4\pi^2 v^2}{p^2}, \\ \hat{\mathbf{x}}_v(s, v) \cdot \hat{\mathbf{x}}_s(s, v) &= 0, \\ \hat{\mathbf{x}}_v(s, v) \cdot \hat{\mathbf{x}}_v(s, v) &= 1, \end{aligned} \right\} \quad (s, v) \in R. \quad (\text{A.1})$$

Similarly, we find that the metric coefficients of a Möbius band \mathcal{B} with parametrization $\hat{\mathbf{y}}$ of the form (5) are given by

$$\left. \begin{aligned} \hat{\mathbf{y}}_s(s, v) \cdot \hat{\mathbf{y}}_s(s, v) &= |\dot{\mathbf{d}}(s)|^2 + 2v\dot{\mathbf{d}}(s) \cdot \dot{\mathbf{g}}(s) + v^2|\dot{\mathbf{g}}(s)|^2, \\ \hat{\mathbf{y}}_s(s, v) \cdot \hat{\mathbf{y}}_v(s, v) &= \dot{\mathbf{d}}(s) \cdot \mathbf{g}(s) + v\mathbf{g}(s) \cdot \dot{\mathbf{g}}(s), \\ \hat{\mathbf{y}}_v(s, v) \cdot \hat{\mathbf{y}}_v(s, v) &= |\mathbf{g}(s)|^2, \end{aligned} \right\} \quad (s, v) \in R. \quad (\text{A.2})$$

A smooth deformation η from \mathcal{H} to \mathcal{B} is isometric if and only if the corresponding metric coefficients of \mathcal{H} and \mathcal{B} satisfy

$$\left. \begin{aligned} \hat{\mathbf{x}}_s(s, v) \cdot \hat{\mathbf{x}}_s(s, v) &= \hat{\mathbf{y}}_s(s, v) \cdot \hat{\mathbf{y}}_s(s, v), \\ \hat{\mathbf{x}}_s(s, v) \cdot \hat{\mathbf{x}}_v(s, v) &= \hat{\mathbf{y}}_s(s, v) \cdot \hat{\mathbf{y}}_v(s, v), \\ \hat{\mathbf{x}}_v(s, v) \cdot \hat{\mathbf{x}}_v(s, v) &= \hat{\mathbf{y}}_v(s, v) \cdot \hat{\mathbf{y}}_v(s, v), \end{aligned} \right\} \quad (s, v) \in R. \quad (\text{A.3})$$

Using (A.1) and (A.2) in (A.3), the directrix \mathbf{d} and generatrix \mathbf{g} of \mathcal{B} must satisfy

$$\left. \begin{aligned} |\dot{\mathbf{d}}(s)|^2 + 2v\dot{\mathbf{d}}(s) \cdot \dot{\mathbf{g}}(s) + v^2|\dot{\mathbf{g}}(s)|^2 &= 1 + \frac{4\pi^2 v^2}{p^2}, \\ \dot{\mathbf{d}}(s) \cdot \mathbf{g}(s) + v\mathbf{g}(s) \cdot \dot{\mathbf{g}}(s) &= 0, \\ |\mathbf{g}(s)|^2 &= 1, \end{aligned} \right\} \quad (s, v) \in R. \quad (\text{A.4})$$

While the first of (A.4) holds only if

$$|\dot{\mathbf{d}}| = 1, \quad \dot{\mathbf{d}} \cdot \dot{\mathbf{g}} = 0, \quad |\dot{\mathbf{g}}| = \frac{2\pi}{|p|}, \quad (\text{A.5})$$

which respectively correspond to (12)_{1,4,5}, the second and third of (A.4) hold only if

$$|\mathbf{g}| = 1, \quad \dot{\mathbf{d}} \cdot \mathbf{g} = 0, \quad (\text{A.6})$$

which respectively correspond to (12)_{2,3}. If, conversely, (A.5) and (A.6) hold, then the matching conditions (A.4) are satisfied. Hence, as claimed in Sect. 2.2, the metric coefficients of \mathcal{H} and \mathcal{B} match if and only if \mathbf{d} and \mathbf{g} satisfy (12).

A.2 First and Second Fundamental Forms

Recalling the definition (43) of J , we see from (A.3) and (A.4) that the first fundamental form I shared by \mathcal{H} and \mathcal{B} is given by

$$I(v) = \begin{bmatrix} J^2(v) & 0 \\ 0 & 1 \end{bmatrix}, \quad (s, v) \in R. \quad (\text{A.7})$$

To calculate the second fundamental form II of \mathcal{B} , we first note from the final form (30) of the parametrization $\hat{\mathbf{y}}$ of \mathcal{B} , the normalization (26) of \mathbf{b} , and the consequence $\mathbf{b} \cdot \dot{\mathbf{b}} = 0$ of differentiating (26) that

$$\begin{aligned} \hat{\mathbf{y}}_s(s, v) \times \hat{\mathbf{y}}_v(s, v) &= \frac{p}{2\pi}(\mathbf{b}(s) \times \dot{\mathbf{b}}(s)) \times \mathbf{b}(s) + v\dot{\mathbf{b}}(s) \times \mathbf{b}(s) \\ &= \frac{p}{2\pi}\dot{\mathbf{b}}(s) - v\mathbf{b}(s) \times \dot{\mathbf{b}}(s), \quad (s, v) \in R. \end{aligned} \quad (\text{A.8})$$

Thus, by the normalization (27) of $\dot{\mathbf{b}}$,

$$|\hat{\mathbf{y}}_s(s, v) \times \hat{\mathbf{y}}_v(s, v)| = J(v), \quad (s, v) \in R, \quad (\text{A.9})$$

and $\bar{\mathbf{n}}$ defined by

$$\bar{\mathbf{n}}(s, v) = -\frac{p}{2\pi J(v)}\dot{\mathbf{b}}(s) + \frac{v}{J(v)}\mathbf{b}(s) \times \dot{\mathbf{b}}(s), \quad (s, v) \in R, \quad (\text{A.10})$$

defines a unit normal to \mathcal{B} at each point on \mathcal{B} . With reference to (18), the choice of sign in (A.10) ensures that $\bar{\mathbf{n}}$ satisfies $\bar{\mathbf{n}}(\cdot, 0) = \mathbf{n}$ on the midline \mathcal{C} of \mathcal{B} . Next, combining (A.10), the further consequences

$$\left. \begin{aligned} \hat{\mathbf{y}}_{ss}(s, v) &= \frac{p}{2\pi} \mathbf{b}(s) \times \ddot{\mathbf{b}}(s) + v \ddot{\mathbf{b}}(s), \\ \hat{\mathbf{y}}_{sv}(s, v) &= \dot{\mathbf{b}}(s), \\ \hat{\mathbf{y}}_{vv}(s, v) &= \mathbf{0}, \end{aligned} \right\} \quad (s, v) \in R, \quad (\text{A.11})$$

(30), the consequence

$$\dot{\mathbf{b}} \cdot (\mathbf{b} \times \ddot{\mathbf{b}}) = -\frac{4\pi^2 k}{p^2} \quad (\text{A.12})$$

of (18), (25), and (35)₁, and the respective consequences $\mathbf{b} \cdot \dot{\mathbf{b}} = 0$ and $\dot{\mathbf{b}} \cdot \ddot{\mathbf{b}} = 0$ of differentiating (26) and (27), we find that

$$\left. \begin{aligned} \bar{\mathbf{n}}(s) \cdot \hat{\mathbf{y}}_{ss}(s, v) &= k(s)J(v), \\ \bar{\mathbf{n}}(s) \cdot \hat{\mathbf{y}}_{sv}(s, v) &= -\frac{p}{2\pi J(v)}, \\ \bar{\mathbf{n}}(s) \cdot \hat{\mathbf{y}}_{vv}(s, v) &= 0, \end{aligned} \right\} \quad (s, v) \in R, \quad (\text{A.13})$$

and, thus, conclude that Π is given by

$$\Pi(s, v) = \begin{bmatrix} k(s)J(v) & -2\pi/pJ(v) \\ -2\pi/pJ(v) & 0 \end{bmatrix}, \quad (s, v) \in R. \quad (\text{A.14})$$

The relations (A.7) and (A.14) are consistent with (42)₁ and (42)₂, respectively.

Supplementary Information The online version contains supplementary material available at <https://doi.org/10.1007/s10659-023-10008-x>.

Acknowledgements The authors express their gratitude for support provided by the Okinawa Institute of Science and Technology Graduate University, funded by the Cabinet Office of the Government of Japan. They also extend their appreciation to Roger Fosdick and two anonymous referees for thoroughly reviewing the initial manuscript and offering valuable comments that enhanced the clarity and presentation of the results.

Author contributions Both authors contributed equally to the work reported in the manuscript.

Declarations

Competing interests The authors declare no competing interests.

Open Access This article is licensed under a Creative Commons Attribution 4.0 International License, which permits use, sharing, adaptation, distribution and reproduction in any medium or format, as long as you give appropriate credit to the original author(s) and the source, provide a link to the Creative Commons licence, and indicate if changes were made. The images or other third party material in this article are included in the article's Creative Commons licence, unless indicated otherwise in a credit line to the material. If material is not included in the article's Creative Commons licence and your intended use is not permitted by statutory regulation or exceeds the permitted use, you will need to obtain permission directly from the copyright holder. To view a copy of this licence, visit <http://creativecommons.org/licenses/by/4.0/>.

References

1. Daigle, M., Miao, D., Lucotti, A., Tommasini, M., Morin, J.F.: Helically coiled graphene nanoribbons. *Angew. Chem., Int. Ed. Engl.* **56**(22), 6213–6217 (2017)
2. Su, F., Zhang, S., Chen, Z., Zhang, Z., Li, Z., Lu, S., Zhang, M., Fang, F., Kang, S., Guo, C., Su, C., Yu, X., Wang, H., Li, X.: Precise synthesis of concentric ring, helicoid, and ladder metallo-polymers with chevron-shaped monomers. *J. Am. Chem. Soc.* **144**, 16559–16571 (2022)
3. Salemme, F.R.: Structural properties of protein β -sheets. *Prog. Biophys. Mol. Biol.* **42**, 95–133 (1983)
4. Fenchel, W.: On the differential geometry of closed space curves. *Bull. Am. Math. Soc.* **57**, 44–54 (1951)
5. Adams, C., Collins, D., Hawkins, K., Sia, C., Silversmith, R., Tshishiku, B.: Duality properties of indicatrices of knots. *Geom. Dedic.* **159**, 185–206 (2012)
6. Koenigs, G.: Sur la forme des courbes à torsion constante. *Ann. Fac. Sci. Univ. Toulouse Sci. Math. Sci. Phys.* **1**, E1–E8 (1887)
7. Călugăreanu, G.: Sur les classes d'isotopie des noeuds tridimensionnels et leurs invariants. *Czechoslov. Math. J.* **11**(4), 588–625 (1961)
8. Kleitman, D.J.: The crossing number of $K_{5,n}$. *J. Comb. Theory* **9**(4), 315–323 (1970)
9. Nocedal, J., Overton, M.L.: Projected Hessian updating algorithms for nonlinearly constrained optimization. *SIAM J. Numer. Anal.* **22**(5), 821–850 (1985)
10. Bauchau, O.A., Trainelli, L.: The vectorial parameterization of rotation. *Nonlinear Dyn.* **32**(1), 71–92 (2003)
11. Schönke, J., Fried, E.: Single degree of freedom everting ring linkages with nonorientable topology. *Proc. Natl. Acad. Sci. USA* **116**(1), 90–95 (2019)
12. Langer, J., Singer, D.A.: Knotted elastic curves in \mathbb{R}^3 . *J. Lond. Math. Soc.* **2**(3), 512–520 (1984)
13. Louie, A., Somorjai, R.: Differential geometry of proteins: a structural and dynamical representation of patterns. *J. Theor. Biol.* **98**(2), 189–209 (1982)
14. Stępień, M., Sprutta, N., Latos-Grażyński, L.: Figure eights, Möbius bands, and more: conformation and aromaticity of porphyrinoids. *Angew. Chem., Int. Ed. Engl.* **50**(19), 4288–4340 (2011)
15. Wallin, S., Zeldovich, K.B., Shakhnovich, E.I.: The folding mechanics of a knotted protein. *J. Mol. Biol.* **368**(3), 884–893 (2007)
16. Liu, L.F., Depew, R.E., Wang, J.C.: Knotted single-stranded DNA rings: a novel topological isomer of circular single-stranded DNA formed by treatment with *escherichia coli* ω protein. *J. Mol. Biol.* **106**(2), 439–452 (1976)
17. Lasters, I., Wodak, S.J., Alard, P., Van Cutsem, E.: Structural principles of parallel beta-barrels in proteins. *Proc. Natl. Acad. Sci. USA* **85**(10), 3338–3342 (1988)
18. Dou, J., Vorobieva, A.A., Sheffler, W., Doyle, L.A., Park, H., Bick, M.J., Mao, B., Foight, G.W., Lee, M.Y., Gagnon, L.A., Carter, L., Banumathi, S., Ovchinnikov, S., Marcos, E., Huang, O.-S., Vaughan, J.C., Stoddard, B.L., Baker, D.: De novo design of a fluorescence-activating β -barrel. *Nature* **561**(7724), 485–491 (2018)
19. Wang, E., He, Z., Zhao, E., Meng, L., Schütt, C., Lam, J.W., Sung, H.H., Williams, I.D., Huang, X., Herges, R., Tang, B.Z.: Aggregation-induced-emission-active macrocycle exhibiting analogous triply and singly twisted Möbius topologies. *Chemistry* **21**, 11707–11711 (2015)
20. Han, D., Pal, S., Liu, Y., Yan, H.: Folding and cutting DNA into reconfigurable topological nanostructures. *Nat. Nanotechnol.* **5**(10), 712–717 (2010)
21. Geng, Z., Xiong, B., Wang, L., Wang, K., Ren, M., Zhang, L., Zhu, J., Yang, Z.: Moebius strips of chiral block copolymers. *Nat. Commun.* **10**(1), 1–9 (2019)
22. Ouyang, G., Ji, L., Jiang, Y., Würthner, F., Liu, M.: Self-assembled Möbius strips with controlled helicity. *Nat. Commun.* **11**(1), 1–9 (2020)
23. Rosengren, K.J., Daly, N.L., Plan, M.R., Waine, C., Craik, D.J.: Twists, knots, and rings in proteins structural definition of the cyclotide framework. *J. Biol. Chem.* **278**(10), 8606–8616 (2003)
24. Craik, D.J., Simonsen, S., Daly, N.L.: The cyclotides: novel macrocyclic peptides as scaffolds in drug design. *Curr. Opin. Drug Discov. Dev.* **5**(2), 251–260 (2002)
25. Jennings, C., West, J., Waine, C., Craik, D., Anderson, M.: Biosynthesis and insecticidal properties of plant cyclotides: the cyclic knotted proteins from *oldenlandia affinis*. *Proc. Natl. Acad. Sci. USA* **98**(19), 10614–10619 (2001)
26. Irobalieva, R.N., Fogg, J.M., Catanese, D.J., Sutthibutpong, T., Chen, M., Barker, A.K., Ludtke, S.J., Harris, S.A., Schmid, M.F., Chiu, W., Zechiedrich, L.: Structural diversity of supercoiled DNA. *Nat. Commun.* **6**(1), 1–11 (2015)
27. Hong, F., Zhang, F., Liu, Y., Yan, H.: DNA origami: scaffolds for creating higher order structures. *Chem. Rev.* **117**(20), 12584–12640 (2017)
28. Maune, H.T., Han, S.P., Barish, R.D., Bockrath, M., Goddard, W.A. III, Rothemund, P.W., Winfree, E.: Self-assembly of carbon nanotubes into two-dimensional geometries using DNA origami templates. *Nat. Nanotechnol.* **5**(1), 61–66 (2010)

29. Zhang, Q., Jiang, Q., Li, N., Dai, L., Liu, Q., Song, L., Wang, J., Li, Y., Tian, J., Ding, B., Du, Y.: DNA origami as an in vivo drug delivery vehicle for cancer therapy. *ACS Nano* **8**(7), 6633–6643 (2014)

Publisher's Note Springer Nature remains neutral with regard to jurisdictional claims in published maps and institutional affiliations.